Persistent Infection of Human Mesenchymal Stromal Cells With Bartonella Henselae Exerts a Proangiogenic Effect

Sara Scutera
University of Turin: Universita degli Studi di Torino https://orcid.org/0000-0002-7431-0875
Stefania Mitola
University of Brescia: Universita degli Studi di Brescia
Rosaria Sparti
Università degli Studi di Torino: Universita degli Studi di Torino
Giorgia Piersigilli
Università degli Studi di Torino: Universita degli Studi di Torino
Elisabetta Grillo
University of Brescia: Universita degli Studi di Brescia
Mattia Bugatti
Università degli Studi di Brescia: Universita degli Studi di Brescia
Valentina Salvi
Università degli Studi di Brescia: Universita degli Studi di Brescia
Daniela Alotto
Azienda Ospedaliero Universitaria Città della Salute e della Scienza di Torino: Azienda Ospedaliero Universitaria Citta della Salute e della Scienza di Torino
Tiziana Schioppa
University of Brescia: Universita degli Studi di Brescia
Tiziana Musso (tiziana.musso@unito.it)
Department of Public Health and Pediatric Sciences, University of Torino, Italy.
Silvano Sozzani
University of Rome La Sapienza: Universita degli Studi di Roma La Sapienza

---

Research

Keywords: Mesemchymal stromal cells, B. henselae, angiogenesis, EGFR, TLR, NOD

Posted Date: December 10th, 2020

DOI: https://doi.org/10.21203/rs.3.rs-122499/v1

TITLE

Persistent Infection of Human Mesenchymal Stromal Cells with *Bartonella henselae* Exerts a Proangiogenic Effect

Scutera Sara[1*] Mitola Stefania[2*] Sparti Rosaria[1] Piersigilli Giorgia[1] Grillo Elisabetta[2] Bugatti Mattia[2] Salvi Valentina[2] Alotto Daniela[3] Schioppa Tiziana[2] Musso Tiziana[1#] Sozzani Silvano[4]

[*] Contributed equally

[#] Corresponding author

Affiliations

[1]Department of Public Health and Pediatric Sciences, University of Torino, Italy.

[2]Department of Molecular and Translational Medicine, University of Brescia, Italy.

[3]Skin Bank, Department of General and Specialized Surgery, A.O.U. Città della Salute e della Scienza, Turin, Italy.

[4]Laboratory Affiliated to Istituto Pasteur Italia-Fondazione Cenci Bolognetti, Department of Molecular Medicine, Sapienza University of Rome, Italy.

Correspondence

Tiziana Musso tiziana.musso@unito.it

ABSTRACT

Background

B henselae is in humans the aetiologic agent of cat-scratch disease and of the vasculoproliferative disorders bacillary angiomatosis and bacillary peliosis. Although endothelial cells are crucial in the pathogenesis other cell types function as reservoir and contribute to pathological angiogenesis. Among them, mesenchymal stromal cells (MSCs) can sense pathogens and mount an appropriate cytokine/chemokine response through different Pattern Recognition Receptors (PRRs). MSCs exert direct antimicrobial effector function but may also shelter bacteria such as M. tuberculosis.

Methods

Adipose-derived MSCs were infected with *B. henselae* and analyzed for bacterial persistence by gentamicin protection assay, immunohistochemistry and immunofluorescence. Involvement of PRRs in bacterial infection was evaluated through gene and protein expression analysis. The effect of infection on MSC proliferation, apoptosis and release of soluble factors was assessed. The role of infected-MSC conditioned medium in promoting Bartonella infection of endothelial cells and angiogenesis was demonstrated using respectively gentamicin protection assay and different pro-angiogenic assays including spheroid, wound healing and morphogenesis.

Results

B. henselae can readily infect MSCs and survive in perinuclear bound vacuoles for up to 8 days. Bartonella infection stimulates MSC proliferation and upregulation of EGFR and of the two pattern recognition receptors (PRRs) TLR2 and NOD1. Specific inhibition of EGFR reduces bacterial internalization and treatment with anti-TLR2 neutralizing antibody or EGFR/NOD1 inhibitors significantly downmodulates CXCL8 production. Secretome analysis shows that, in addition to CXCL8, infected MSCs secrete higher levels of the proangiogenic factors VEGF, FGF-7, MMP-9, PIGF, serpin E1, TSP-1, uPA, IL-6, CCL5 and PDGF-D. Importantly, supernatants from *B. henselae*-infected MSCs increase the susceptibility of ECs to *B. henselae* infection while enhancing

EC proangiogenic potential.

Conclusions

Altogether, these findings indicate that MSCs constitute a novel niche for *B. henselae*, which favors the persistence of vascular proliferative disorders.

KEYWORDS

Mesemchymal stromal cells, *B. henselae*, angiogenesis, EGFR, TLR, NOD

BACKGROUND

Endemic among domestic cats, *B. henselae* is a fastidious gram-negative bacterium that, in humans, can cause subclinical intraerythrocytic bacteremia, mainly transmitted by cat fleas. In immunocompetent individuals, *B. henselae* infection can also lead to cat-scratch disease (CSD), characterized by lymphadenopathy with suppurative granulomas. Atypical clinical presentations of CSD, ranging from prolonged fever of unknown origin to hepatosplenic, ocular and neurological manifestations, have also been reported [1].

Individuals unable to mount an immune response against *B. henselae* tend to develop a tumor-like vascular proliferative response in the skin and/or internal organs, which can lead to bacillary angiomatosis (BA) or bacillary peliosis (BP) [2]. Interestingly, *B. henselae* survive in human endothelial cells (ECs) and stimulate their migration, proliferation and secretion of various proinflammatory and proangiogenic factors, such as ICAM-1, angiopoietin-2, IL-8 and MCP-1 [2–5]. In addition, other cells types, such as monocytes/macrophages [6] are recruited to the vasoproliferative lesions where they stimulate EC proliferation in a paracrine manner through VEGF and IL-8 secretion [7]. Moreover, macrophages and DCs localized in the skin at the site of infection–play a role in transporting *Bartonella* species to endothelium [7]. Of note, mononuclear phagocytes, $CD34^+$ progenitor cells and ECs can provide an infection reservoir from which *B. henselae* periodically reaches the bloodstream and disseminates within the host [8]. Despite the

clinical implications of protracted *Bartonella* infections, the underlying mechanism of intracellular *B. henselae* persistence is poorly understood, and the existence of different reservoirs still remains to be determined.

Mesenchymal stem cells (MSCs) are multipotent adult stem cells present in various tissues, including the bone marrow and the adipose tissue, which have recently received much attention due to their regenerative potential and immunomodulatory properties [9]. In addition, MSCs modulate the tissue vascularization both through direct contact and indirect signaling [10,11].

A diverse and multitasking role of MSCs during bacterial infection has recently emerged [12,13]. MSCs can sense pathogens and mount an appropriate cytokine/chemokine response through Toll-like receptors (TLRs), NOD-like receptors (NLRs) and the scavenger receptors MARCO and SR-B1 [12]. Moreover, MSCs express EGFR, a (member of the ErbB receptor tyrosine kinase family), shown to enhance their proliferation and the release of angiogenic factors [14]. Interestingly, ErB receptors can be exploited by a wide range of microbes to facilitate their cellular entry and subvert host immunity [15]. However, despite the emerging role of MSCs in infectious diseases, the mechanisms regulating the interplay between MSCs and bacteria are yet to be defined. MSCs exert antimicrobial effects by secreting antimicrobial peptides (AMPs) and expressing the anti-inflammatory factor indoleamine2,3-dioxygenase (IDO)[16,17]. Furthermore, MSC administration appears to reduce pathogen burden in animal models of polymicrobial sepsis and pneumonia [18–21]. On the other hand, MSCs serve as a niche where *M. tuberculosis* can survive and persist during antimicrobial therapy. Indeed, viable *M. tuberculosis* was recovered from MSCs infiltrating TB granulomas in humans and in a tuberculosis mouse model [22,23]. Thus, it is likely that other pathogens, besides *M. tuberculosis*, known to cause chronic infections, may similarly exploit MSCs to favor their persistence in the host.

In this study, we show that *B. henselae* can readily infect human MSCs and survive in these cells for a prolonged period, promoting the release of proinflammatory and proangiogenic factors through a novel signaling pathway involving TLR2, NOD1 and EGFR.

METHODS

Reagents and antibodies. MTT 3-(4,5-dimethylthiazol-2-yl)-2,5-diphenyltetrazolium bromide was purchase from Sigma Aldrich (MO, USA). The EGFR inhibitor gefitinib and RIPK2 inhibitor GSK583 were purchase from MedChemExpress (NJ, USA). The neutralizing antibody anti-TLR2 (anti-human TLR2-IgA, clone B4H2) and the human IgA2 Isotype control were both purchased from InvivoGen (CA, USA). The neutralizing antibody anti-EGFR (mouse IgG1, clone LA1) and its specific isotype control were from EMD Millipore Corporation (CA, USA). Recombinant human VEGF-A_{165} and EGF were from R&D System (MN, USA). The Protease Inhibitor Cocktail and the Phosphatase Inhibitor Cocktail were from Sigma Aldrich. The rabbit poly anti–*B. henselae* monoclonal antibody (anti-*BH*; mouse IgG2b/clone H2A10) was purchased from Abcam (Cambridge, United Kingdom), whereas the biotinylated secondary IgG antibodies were from Agilent (CA, USA). The antibodies against EGFR (clone A10, sc-373746), pY1068-EGFR (sc-377547) and secondary antibodies HRP-conjugated were from Santa Cruz Biotechnology, Inc. (Texas, USA). The wheat germ agglutinin-Alexa Fluor 594 or 488 conjugate, Alexa Fluor® 594 phalloidin (A12381), goat anti-Mouse Alexa Fluor® 488 conjugate, goat anti-Rabbit Alexa Fluor® 594 conjugate and DAPI (4',6-diamidin-2-fenilindolo) were all from ThermoFisher Scientific (CA, USA). The anti-human TLR-2 FITC (mouse IgG2a) and anti-human TLR-4 PE (mouse IgG2a) or respective isotype control were from BioLegend (CA, USA).

Cell culture. Human MSCs were isolated from adipose tissues as previously described [24]. Human adipose tissues were collected by lipoaspiration from healthy donors after written consent and in compliance with the Declaration of Helsinki and the local Ethic Committee (Comitato Etico Interaziendale A.O.U. Città della Salute e della Scienza di Torino - A.O. Ordine Mauriziano - ASL TO1, No. 0009806). Subsequently, MSCs were analyzed by flow cytometry to verify their phenotype was positive for CD73, CD90 and CD105 and negative for CD11b, CD34 and CD45.

HUVECs were isolated from umbilical cords of healthy informed volunteers in compliance

with the Declaration of Helsinki. HUVECs were used at early (I-IV) passages and grown on culture plates coated with porcine gelatin in M199 medium (Gibco Life Technologies, ThermoFisher Scientific Group) supplemented with 20% heat-inactivated fetal calf serum (FCS, Gibco Life Technologies), endothelial cell growth factor (ECGF) (10 µg/mL), and porcine heparin (100 µg/mL) (Sigma Aldrich) (100 µg/mL) or in complete EBM2 medium (Lonza Group Ltd Basel, Switzerland).

Bacterial cultures. *B. henselae* Houston I strain (ATCC 49882; Manassas, VA, USA) was grown on 5% sheep blood Columbia agar plates (BioMerieux, Lyon, France) under anaerobic conditions (i.e., candle jar) at 37°C for 10 days. Bacteria were harvested under a laminar-flow hood by gently scraping colonies off the agar surface. They were then suspended in MICROBANK™ cryopreservative solution and stored at -80°C in 1-mL aliquots. For biological assays, frozen bacteria were incubated in Schneider's Insect Medium (Sigma-Aldrich) supplemented with 10% FBS at 37°C and 5% CO_2 for 6 days. Spectrophotometry was performed to evaluate bacterial growth [optical density (OD600) 0.6, corresponding to $1x10^8$ bacteria/mL] and confirmed by plating serial dilutions on 5% sheep blood Columbia agar plates. Bacteria, washed 3 times with 1X PBS, were then added to cell cultures. Where indicated, *B. henselae* were killed by heating thawed bacteria at 56°C for 30 min.

Infection assay. *B. henselae* invasion of MSCs was assessed by GPA. Briefly, 12,500 cells/cm^2 MSCs were seeded for 24 h in RPMI supplemented with 10% FCS. To compare MSCs with HUVECs, infection was carried out with 60,000 cells *per* well seeded in DMEM 10% FCS or complete EBM2 medium (Lonza Group Ltd), respectively. The next day, cells were washed twice and cultured in RPMI supplemented with 10% FCS without antibiotics. *B. henselae* (MOI 10-50-100) was added to the cells, immediately centrifuged at 1200 g for 5 min to allow the association of bacteria with the cellular surface, and incubated for 1, 2, 3, 4 and 8 days. At the end of infection period, gentamicin sulfate (Sigma-Aldrich) (100 µg/mL) was added to the medium for 2 h to kill all extracellular bacteria—this assay was performed in triplicate, and control wells were left

uninfected. Cells were then washed extensively and lysed by the addition of 200 µL of distilled water for 5 min and sonicated for 1.30 min. Lysates were serially diluted, plated on Columbia blood agar, and CFUs were counted after 1 week of incubation. To determine intracellular survival after 96 h of infection, extracellular bacteria were killed by gentamicin treatment for 2 h. Cells were further incubated in normal medium for the remaining time of the indicated infection period. When indicated, cells were pretreated for 6 h with the specific inhibitors gefitinib (10 µM) and GSK583 (1 µM) or with a specific antibody against EGFR or its corresponding isotype control antibody at 10 µg/ml. GPA was performed as described above after 1 or 2 days. In some experiments, HUVECs were cultured in the presence of CM from untreated and infected MSCs.

Immunostaining. MSCs (1×10^4) were seeded on coverslips and infected with *B. henselae* at a MOI of 100. Cells were fixed in methanol and sequentially incubated with blocking solution (0.1% BSA in PBS) for 15 min, rabbit poly anti-*B henselae* monoclonal antibody (1:50) for 1 h and biotinylated secondary IgG antibodies for 30 min. Samples were then stained with horseradish peroxidase streptavidin (HRP Streptavidin) or with the chromogen DAB (3, 3'-diaminobenzidine) (ThermoFisher Scientific).

For immunofluorescence analysis, MSCs were seeded at 0.25×10^4 on coverslips, infected with *B. henselae* (MOI 100), fixed in 3.75% PBS-buffered paraformaldehyde (PFA), and permeabilized with 0.25% saponin, 5% normal goat serum, and 2% serum bovine albumin in 1X PBS. Cells were then stained with the indicated antibodies in the presence of 0.25% saponin.

Cells were analyzed under a Zeiss Observer.Z1 epifluorescence microscope equipped with a Plan-Apochromat 100×/1.4 NA oil objective and ApoTome2 imaging system for optical sectioning. Z-stack images were elaborated through AxioVision 3D and Extended Focus modules.

Immunoblotting. Total cell lysates were prepared in cold lysis buffer (1% Triton X-100, 1% NP-40 in PBS, pH 7.4) containing a cocktail of protease and phosphatase inhibitors (Sigma-Aldrich). Samples (10-20 µg) were analyzed by 10% SDS-PAGE under denaturing conditions, followed by Western blotting, using the indicated antibodies. Chemiluminescent signal (Clarity

Western ECL Substrate, Bio-Rad) was acquired by ChemiDoc™ Imaging System (BioRad).

Real-time PCR. Total MSC RNA isolated with the Qiagen RNeasy mini kit was treated with DNase I (Qiagen, Hilden, Germany) and retrotranscribed into cDNA by iScript cDNA Synthesis Kit (Bio-Rad Laboratories Inc., Hercules, CA, USA). Gene specific primers were: TLR-2 (sense, 5'- CTCATTGTGCCCATTGCTCTT -3'; antisense, 5'- TCCAGTGCTTCAACCCACAAC -3'), TLR-4 (sense, 5'- GGCCATTGCTGCCAACAT -3'; antisense, 5'- CAACAATCACCTTTCGGCTTTT -3'), Bax (sense, 5'- AGAGGATGATTGCCGCCGT -3'; antisense, 5'- CAACCACCCTGGTCTTGGATC -3'), Bcl-2 (sense, 5'- TGCA.CCTGACGCCCTTCAC -3'; antisense, 5'- AGACAGCCAGGAGAAATCAAACAG -3'), HPRT (sense, 5'- TGACCTTGATTTATTTTGCATACC -3'; antisense, 5'- CGCTTTCCATGTGTGAGGTGATG -3'), RPL13A (sense, 5'-CATAGGAAGCTGGGAGCAAG-3'; antisense, 5'- GCCCTCCAATCAGTCTTCTG-3'). For EGFR, NOD1 and NOD2, validated primers from Bio-Rad were used (Unique Assay ID qHsaCID0007564, qHsaCED0005079 and qHsaCED0056944 respectively). For quantitative real-time PCR, the iQTM SYBR Green Supermix (Bio-Rad Laboratories Inc., Segrate, MI, Italy) was used according to the manufacturer's instructions. Reactions were run in duplicate on a CFX96 Real Time System and analyzed by BioRad CFX Maestro Software (Bio-Rad Laboratories Inc.). Gene expression was normalized to HPRT or RPL13A mRNA content.

MTT assay. MSC cell viability was measured by MTT 3-(4,5-dimethylthiazol-2-yl)-2,5-diphenyltetrazolium bromide assay. Cells were seeded at a density of $2x10^3$/well in 96-well plates. After 24 h of incubation in RPMI 10% FBS without antibiotics, cells were infected with *B. henselae* (MOI 100). The medium was changed after 4 days to wash out all extracellular bacteria. When indicated, cells were treated with heat-killed *B. henselae*. Cells were then incubated for 3 h with 20 µl MTT (final concentration 0,5 mg/ml). Formazan crystals were solubilized for 10 min in 100 µl DMSO, and OD 570 nm was measured using a microplate reader (VICTOR3™, PerkinElmer, MA,

USA).

Annexin V Assay. MSCs untreated or infected for 96 h with *B. henselae* were stained with annexin V-FITC and PI (Sigma Aldrich) according to the manufacturer's instructions. Samples were analyzed by FACS Calibur (Becton Dickinson), and results were quantified using FlowLogic (Miltenyi Biotec, Bergisch Gladbach, Germany).

Flow cytometry. MSCs were collected at the indicated times after infection and preincubated for 30 min at 4°C in 1X PBS supplemented with 2% goat serum and 0.2% sodium azide, washed twice with 1% bovine serum albumin (BSA). Successively, cells were incubated for 30 min at 4°C with anti-human TLR-2 FITC, anti-human TLR-4 PE or control isotypes. Flow cytometry analysis was performed using FACS Calibur and FlowLogic as described above.

Cytokine measurements. MSCs seeded in 24-well plates were infected with a MOI of 100 for the indicated times. For some experiments, cells were pretreated with the pharmacological inhibitors gefitinib and GSK583 or the neutralizing antibody anti-TLR2. Cell-free supernatants were then harvested to measure human VEGF-A, CXCL8, IL-6 and CCL5 production by ELISA (R&D Systems, Minneapolis, MN, USA). To quantify human PDGF-D, a specific kit from Elabscience (Wuhan, Hubei, P.R.C) was employed.

Preparation of conditioned medium. MSCs, cultured into 12-well plates at a density of 0.5×10^5 cells/well in RPMI 10% FBS without antibiotics, were left untreated or infected for 96 h with *B. henselae*. Cells were then extensively washed to remove extracellular bacteria, and fresh RPMI was replaced for 72 h. Conditioned medium was collected, centrifuged at 4000 rpmi for 10 min and then filtered, aliquoted, and stored at -20°C.

Angiogenesis array. The human angiogenesis array (Proteome Profiler™ Array; R&D Systems) was used to assess the expression of 55 angiogenic-related proteins in MSCs uninfected or infected with *B. henselae* for 96 h. The array membranes were probed with pooled supernatants derived from three independent experiments. Enhanced chemiluminescence was used to detect protein binding to the antibody array, followed by exposure to an X-ray film. The signal intensity of

each antigen-specific antibody spot was quantified using Fiji-ImageJ (NIH) software. For comparison of the relative expression of proteins in uninfected *vs* infected cells, the mean pixel density of the pair of duplicate spots for each protein, after subtraction of the mean pixel density of the negative control spots of the respective array, was normalized to the mean pixel density of the positive control spots. Heat map analysis using the normalized data was performed by GraphPad PRISM 8.0 software.

Sprouting assay. Sprouting of HUVEC spheroids was assessed as described previously [25]. Briefly, spheroids were prepared in 20% methylcellulose medium, embedded in a fibrin gel and stimulated with recombinant human VEGF-A (30 ng/mL) or with different concentrations of CM from uninfected or infected MSCs. The number of radially growing cell sprouts was counted after 24 h using an Axiovert 200M microscope equipped with LD A Plan 20X/0.30PH1 objective (Carl Zeiss) and expressed as relative increase over untreated spheroids.

Motility assay. HUVEC motility assay was based on "scratch" wounding of a confluent monolayer. Briefly, HUVECs (1×10^5) were seeded onto 0.1 % collagen type I (BD Biosciences, Italy)-coated six-well plates in complete medium until a confluent monolayer was formed. The cell monolayers were scratched using a pipette tip, washed with 1X PBS to remove the undetached cells and treated with MSC conditioned medium. After 24 h, cells were photographed under an Axiovert 200M microscope (Carl Zeiss) equipped with LD A Plan 20X/0.30PH1. The healed area was quantified through computerized analysis by subtracting the wound area at 24 h from the initial area.

Tube formation assay. EC vessel formation was assessed by tube morphogenesis assay in a three-dimensional (3D) collagen matrix. To this end, HUVECs were seeded onto Reduced Growth Factor Basement Membrane Matrix Cultrex® (BME) (Trevigen, Italy)-coated µ-slide angiogenesis chamber (Ibidi, Martinsried, Germany) at a density of $4.0x10^4$ cells/cm^2 in the absence or presence of CM from untreated or infected MSCs. After 48 h, cells were photographed using an Axiovert

200M microscope, and the number of meshes/field was counted.

Statistical Analysis. Statistical significance was determined by non-parametric Student's t-test and one-way analysis of variance followed by Tukey's multiple-comparison test. Results were analyzed by GraphPad PRISM 8.0 software (CA, USA).

RESULTS

***B. henselae* invades and persists in MSCs**. To characterize the interaction of MSCs with *B. henselae,* adipose-derived MSCs were infected with MOI of 100:1 for 1, 2, 3, 4 and 8 days and then treated with gentamicin to kill all residual extracellular bacteria. Subsequently, the number of viable intracellular bacteria was measured by colony-forming unit (CFU) assay. The number of *B. henselae* invading MSCs increased progressively over a 3-day period and the number of CFUs in MSCs remained unchanged up to 8 days ($P < 0.05$) (Fig. 1A). At day 8 post-infection (pi), the vast majority of MSCs contained *B. henselae*, as demonstrated by the strong cytoplasmic reactivity of an anti-*B. henselae* monoclonal antibody (anti-BH) (Fig. 1B). As expected, at lower MOIs, we observed a reduction in the number of viable intracellular bacteria. At a MOI 10:1 after 1 day of infection, about 30 bacteria *per* 100 cells were detected (data not shown). To obtain a sufficient number of intracellular bacteria for proper readout, subsequent studies were thus carried out at an MOI of 100.

To assess *B. henselae* intracellular survival after the initial infection and gentamicin treatment, MSCs were cultured in medium without gentamicin for four additional days. The number of viable intracellular bacteria recovered, which remained stable during the first 96 h, was significantly lower at day 8 compared to day 4 (Fig. 1C). The ability of *B. henselae* to invade MSCs was further assessed by comparing its infection efficiency in MSCs *vs* HUVECs, a known target of *B. henselae* infection. The number of intracellular bacteria recovered after 24 h of infection from MSCs was significantly higher than that recovered from HUVECs (Fig. 1D).

Next, we followed MSC infection by fluorescence microscopy. At day 1 pi, *B. henselae*—stained with DAPI (Cyan)—remained mainly anchored to the MSC membrane, with only a few bacteria present in the cytoplasm (Fig. 2A, upper right panel, arrowhead). From day 2 pi onward, the number of internalized bacteria increased, and a significant amount of *B. henselae* localized in perinuclear vesicles (Fig. 2A, lower left and central panel, thin arrows). After 8 days pi, the bacteria aggregated and co-localized with F-actin in globular structures called invasomes, first described in *Bartonella*-infected ECs (Fig. 2A, lower right panel, large arrow; and Fig. 2B) as attested by 3D immunofluorescence analysis. By contrast, from day 2 to day 8, a significant amount of bacteria entered individually or in the form of small aggregates, leading to the formation of *Bartonella*-containing vacuoles (BCVs), mainly localized in the perinuclear compartment.

Altogether, these findings indicate that *B. henselae* is internalized by MSCs—even more efficiently than HUVECs—where it can persist for a prolonged time in a quiescent state.

***B. henselae* infection enhances MSC proliferation.** We next asked whether *B. henselae* infection would affect MSC survival. *B. henselae* infection did not induce cell death in MSCs as demonstrated by similar amounts of Annexin V positive cells found in uninfected *vs* infected MSCs (Fig. 3A). This finding was further supported by the unaltered *Bcl-2* (antiapoptotic) /*Bax* (apoptotic) expression ratio observed in these cells (Fig. 3B). We then assessed the effect of infection on the proliferation rate of MSCs. Infected-MSCs grew significantly faster compared to their uninfected counterparts. Conversely, heat-inactivated *B. henselae* (HKB.h.) failed to enhance MSC proliferation (Fig. 3C).

Role of TLR2, EGFR and NOD1 in MSC infection with *B. henselae*. As TLR, NOD and EGFR are involved in pathogen/host cell interactions [26], we next assessed the expression of these receptors in response to *B. henselae* infection. Interestingly, *B. henselae* infection led to a more than 6-fold increase in TLR2 expression at both mRNA and protein level, while TLR4 expression remained basically unchanged (Fig. 4A and 4B). Furthermore, RT-PCR analysis showed a

significant upregulation of NOD1 mRNA at day 2 and 4 pi (Fig. 4A). NOD2 gene expression was not detected in uninfected or infected MSCs. Lastly, *B. henselae* infection significantly increased EGFR mRNA and phosphorylation levels (Fig. 4A and 4C, respectively). Specifically, we detected increased phosphorylation as early as 30 min pi, which remained above basal levels up to 120 min pi (Figure 4C).

The involvement of these receptors was evaluated in the production of CXCL8, a cytokine shown to be triggered by *Bartonella* in different cell types [27], *Bartonella* infection of MSCs enhanced their ability to produce CXCL8, which was neutralized by incubation with an anti-TLR2 neutralizing antibody (Fig. 4D). Similarly, treatment with the EGFR inhibitor gefitinib or with the selective RIP2K inhibitor GSK583 significantly reduced the release of CXCL8 in *B. henselae*-infected MSCs (Fig. 4D), suggesting that the EGFR/NOD pathway may play a role in CXCL8 transcriptional regulation. Finally, to address the role of bacterium-activated EGFR in *Bartonella* entry, we treated MSCs with the EGFR inhibitor gefitinib and a neutralizing anti-EGFR antibody, detecting a reduced bacterial internalization by about 70% and 50%, respectively, compared to untreated cells (Fig. 4E).

***B. henselae*-infected MSCs promote angiogenesis and infection of endothelial cells.** Since MSCs regulate vascular remodeling and angiogenesis [28], we assessed the pro-angiogenic activity of conditioned medium (CM) from *B. henselae*-infected MSCs. To this end, CM from uninfected or *B. henselae*-infected MSC cultures were tested in a scratch wound healing assay using HUVECs. CM from *B. henselae*-infected MSCs (CM-MSC *B. henselae*), induced a more rapid repair of HUVECs monolayer (Fig. 5A). In addition, the CM-MSC *B. henselae* was 9 fold more powerful then CM of uninfected MCS (CM-MSC CTRL) on a spheroid-based sprouting assay, which faithfully recapitulate the proliferation, invasion and reorganization in tube-like structure of ECs (Fig. 5B). In keeping with the pro-angiogenic activity of MSCs, the CM-MSC CTRL induced the formation of radial sprouts, similarly to what induced by spheroids stimulation with 30 ng/mL of VEGF-A (Fig. 5B, right panel). Importantly, CM-MSC *B. henselae* but not that from uninfected

cells (CM-MSC CTRL) accelerated the morphogenesis of HUVECs when seeded on Cultrex Extracellular Matrix, as judged by the number of closed structures formed at 18 h pi (Fig. 5C).

Even though ECs and MSCs can crosstalk through soluble mediators [29], there is no data on the effects of MSC on the susceptibility of ECs to bacterial infection. We thus assessed the extent of *Bartonella* internalization, at day 1 pi, in HUVECs pretreated with CM from uninfected MSCs or *B. henselae*-infected MSCs. While there were no differences in the yield of bacteria between control HUVECs (Ctrl) and HUVECs pretreated with CM-MSC CTRL, a significantly higher number of bacteria was detected in HUVECs pretreated with CM-MSC *B. henselae* (Fig. 5D).

Angiogenic expression profile of *B. henselae*-infected MSCs. Finally, we assessed the impact of *B. henselae* infection on the ability of MSCs to modulate the expression of pro-inflammatory and pro-angiogenetic molecules. For this purpose, we probed an antibody angiogenesis array with CM from uninfected and 4-day-infected MSCs. Among the 55 proteins of the assay, 27 were detected in CM of both uninfected and infected MSCs. Densitometric analysis showed the upregulation of FGF-7, CXCL8, MMP-9, PIGF, Serpin E1, TSP-1, uPA and VEGF, in *B. henselae*-infected MSCs CM compared to those from uninfected MSCs (Fig. 6A). Intriguingly, activin A was the only growth factor downregulated in *B. henselae*-infected MSCs (Fig. 6A). Of note MCP-1, PTX3 and TIMP-1 were all highly expressed but remained unchanged following infection (Fig. 6A, 6B and Suppl. Fig. S1, Additional File 1). The quantification by ELISA of the increased production of CXCL8 and VEGF in the supernatants of MSCs infected for 1, 4 and 7 days was in good agreement with the array data (Fig. 6C). Finally, other molecular factors known for their angiogenic activity, but not included in our array, such as IL-6, CCL5 and PDGF-D, were also induced following *B. henselae* infection (Fig. 6C).

DISCUSSION

Bartonella spp exploits several mechanisms to hide inside erythrocytes and endothelial cells (ECs) to evade immune responses and persist in both animal reservoir and human host. Numerous

361 evidence indicate that the blood-stage phase is preceded by the infection of cellular niches that
362 periodically release bacteria able to invade erythrocytes. ECs were the first cell types considered a
363 primary niche as they support *Bartonella* replication and reside in proximity to the bloodstream
364 [2,30]. However, later studies identified additional *Bartonella* persistence sites including
365 hematopoietic progenitor cells and dendritic cells [8,31].

366 In this study we provide evidence showing that once inside *B. henselae* resides in MSCs
367 without proliferating for several days. *Bartonella* localizes in numerous perinuclear membrane
368 bound vacuoles, as previously shown in HUVECs and MonoMac cells [32,33], or at late time points
369 of infection, as aggregated bacteria enclosed into F actin-rich cell membrane protrusions identified
370 as invasome structures [34].

371 MSCs sense microorganisms trough the expression of various PRR including Toll-like
372 receptors (TLRs) and Nod-like receptors (NLRs). The engagement of such receptors modulate MSC
373 functions and their abilities to secrete cytokines [35]. Our studies revealed that TLR2, NOD1 and
374 EGFR are involved in the recognition and responses to *Bartonella* by MSCs. We show that, upon
375 infection with *B. henselae*, MSCs secret large amounts of CXCL8, which is curbed by incubation
376 with an anti-TLR2 antibody. A central role of TLR2 signaling during *Bartonella* infection is
377 consistent with previous findings indicating that *B. henselae*, despite being Gram-negative,
378 preferentially activates TLR2 [31]. In infected cells, NOD1 and NOD2 recognize bacterial
379 peptidoglycan derivatives released into the cytosol and, upon ligand association with the adaptor
380 protein receptor-interacting-serine/threonine-protein kinase 2 (RIPK2 or RIP2), trigger
381 proinflammatory signaling [36]. In our experimental system, inhibition of the RIP2 with the highly
382 RIPK2-specific compound GSK583[37] decreased CXCL8 release, indicating that NOD1 activation
383 and signaling through RIP2 during MSC infection is, in part, responsible for inducing the
384 inflammatory response to *B. henselae* infection. Consistent with our results, NOD1 mediates
385 CXCL8 induction after recognition of *Helicobacter pylori*, *Escherichia coli* [38,39] and *Chlamydia*
386 *pneumoniae* [40]. Importantly, we also show that gefitinib, an inhibitor of EGFR tyrosine kinase

387 domain, used to treat various forms of cancer, can hamper *B. henselae*-mediated induction of
388 CXCL8, suggesting a role of EGFR in this pathway. Gefitinib also exerts an off-target inhibitory
389 activity on the expression of RIP2 [41], thus the inhibition of CXCL8 secretion may be due to
390 blockage of NOD/RIP2 signaling alongside that of EGFR. In support to this hypothesis,
391 EGFR/NOD cooperation has been recently involved in cytokine production in dengue virus infected
392 monocytes [42]. Moreover, a growing body of literature highlights the importance of EGFR/ErbB
393 in several bacterial and viral inflammatory responses [15,43] and in pathogenic angiogenesis [44].
394 In addition to stimulation of EGFR tyrosine kinase phosphorylation, *Bartonella* also enhanced
395 EGFR mRNA expression suggesting that this upregulation could serve as a positive feedback
396 system. A functional role of EGFR signaling in the immune response against *B. henselae* is further
397 supported by the observation that treatment of MSCs with the kinase inhibitor gefitinib or an anti-
398 EGFR antibody significantly decreases *Bartonella* internalization. In this regard, EGFR has been
399 recently shown to act as a cofactor in mediating pathogen internalization in host cells (e.g., HBV,
400 HCV, Chlamydia and Candida) [15]. Our finding indicates an important role of EGFR activation in
401 *Bartonella* invasion; however, as these EGFR inhibitors do not completely abrogate *Bartonella*
402 uptake by MSCs, it is likely that other receptors, other than EGFR, may play a role in *Bartonella*
403 infection. Moreover, it remains to be investigated whether EGFR activation is due to the direct
404 interaction of *Bartonella* with the EGFR extracellular domain or by its transactivation by EGFR
405 ligands (i.e., EGF, HBEGF, TGFα, BTC, AREG, EREG and EPGN) [42] as shown for *H. pylori*
406 and *Neisseria* spp. [45,46]. EGFR signaling pathways exert an antiapoptotic activity in
407 *Pseudomonas*- and *Helycobacter*- infected cells [47,48] suggesting that EGFR activation by
408 *Bartonella* promotes the survival and proliferation of infected MSCs.

409 These effects may also be explained at least in part by the robust release of cytokine/growth
410 factors caused by *Bartonella* infection. In addition to CXCL8, angiogenic factors upregulated in
411 infected MSCs include FGF-7, MMP-9, PIGF, serpin E1, TSP-1, uPA, IL-6, CCL5 and VEGF,
412 leading to the induction of a pro-angiogenic phenotype in ECs as well as an increased susceptibility

of ECs to infection. Data reporting a role of MSCs in facilitating the infection of other cell types are sparse and concern mainly phagocytic cells. MSCs enhance bacterial uptake by PMNs, resulting in enhanced clearance of bacteria [49], and mediate the reactivation of HIV in monocytic cells [50]. The secretion of factors by infected MSCs, acting in a paracrine fashion, may stimulate the infection of ECs allowing bacterial persistence. Consistent with the fact that ECs are not the major cell type producing VEGF [32] *Bartonella*-triggered angiogenesis has been shown to be supported by VEGF and CXCL8 released by macrophages infiltrating the lesions [8]. Since MSCs are recruited at the sites of infection/inflammation, just in contact with ECs [29,51], we propose that infected MSCs might support the angiogenic loop by releasing high levels of pro-angiogenic factors. A role of MSCs can be envisioned in different scenarios of *Bartonella* infections. MSC are recruited around the granuloma of lymph node tuberculosis to establish a persistent infection and likely to suppress T cell response [52]. Moreover, MSC have been also found in oral pyogenic granuloma tissues [53]. Granulomatous lymphadenitis is the pathological hallmark of cat scratch disease whereby MSCs could also be hired in *Bartonella* granuloma to contribute to the immune pathogenesis. The crosstalk between MSCs and ECs is well characterize in the bone marrow where it collaborates in the maintenance of the hematopoietic stem cell niche and regulates emergency myelopoiesis during infection [54]. Interestingly MSCs have been shown to regulate proliferation and erythroid differentiation of $CD34^+$ stem cells [55]. As *B. henselae* can infect $CD34^+$ bone marrow progenitor cells, bone marrow has been proposed as one of the potential niches. Moreover multifocal bone marrow involvement has been shown in CSD [56,57] and a contribution of *B. henselae* infection to ineffective erythropoiesis has been suggested [58]. *Bartonella*-infected MSCs releasing soluble molecules can recruit and activate ECs which in turn collaborate with MSCs in the fine regulation of the hematopoietic stem cell niche.

CONCLUSIONS

In conclusion, this study provides novel insights into the role of MSCs in serving as a bacterial reservoir during *B. henselae* infection and identifies TLR2, NOD1 and EGFR as the

receptors involved in the recognition of *B. henselae*. Moreover, *B. henselae* triggers a potent proangiogenic effect, which activates ECs and at the same time enhances their susceptibility to bacterial infection. Thus, a better understanding of the involvement of MSCs in *Bartonella*-induced angiogenesis will allow the development of targeted therapeutic strategies for the treatment of vascular proliferative disorders.

Abbreviations

MSCs: mesenchymal stromal cells

ECs: endothelial cells

DCs: dendritic cells

TLRs: Toll-like receptors

NLRs: NOD-like receptors

PRRs: Pattern Recognition Receptors

CSD: cat scratch disease

BA: bacillary angiomatosis

BP: bacillary peliosis

GPA: gentamicin protection assay

CM: conditioned medium

MOI: multiplicity of infection

ANOVA: analysis of variance

REFERENCES

1. Florin TA, Zaoutis TE, Zaoutis LB. Beyond Cat Scratch Disease: Widening Spectrum of Bartonella henselae Infection. Pediatrics. American Academy of Pediatrics; 2008;121:e1413–25.

2. Harms A, Dehio C. Intruders below the Radar: Molecular Pathogenesis of Bartonella spp. Clin Microbiol Rev. 2012;25:42–78.

3. McCord AM, Burgess AWO, Whaley MJ, Anderson BE. Interaction of Bartonella henselae with Endothelial Cells Promotes Monocyte/Macrophage Chemoattractant Protein 1 Gene Expression and Protein Production and Triggers Monocyte Migration. Infect Immun. 2005;73:5735–42.

4. Berrich M, Kieda C, Grillon C, Monteil M, Lamerant N, Gavard J, et al. Differential Effects of Bartonella henselae on Human and Feline Macro- and Micro-Vascular Endothelial Cells. Bruggemann H, editor. PLoS ONE. 2011;6:e20204.

5. Tsukamoto K, Shinzawa N, Kawai A, Suzuki M, Kidoya H, Takakura N, et al. The Bartonella autotransporter BafA activates the host VEGF pathway to drive angiogenesis. Nat Commun. 2020;11:3571.

6. Musso T, Badolato R, Ravarino D, Stornello S, Panzanelli P, Merlino C, et al. Interaction of Bartonella henselae with the Murine Macrophage Cell Line J774: Infection and Proinflammatory Response. Clements JD, editor. Infect Immun. 2001;69:5974–80.

7. Resto-Ruiz SI, Schmiederer M, Sweger D, Newton C, Klein TW, Friedman H, et al. Induction of a Potential Paracrine Angiogenic Loop between Human THP-1 Macrophages and Human Microvascular Endothelial Cells during Bartonella henselae Infection. Infect Immun. 2002;70:4564–70.

8. Mändle T, Einsele H, Schaller M, Neumann D, Vogel W, Autenrieth IB, et al. Infection of human CD34+ progenitor cells with Bartonella henselae results in intraerythrocytic presence of B henselae. Blood. 2005;106:1215–22.

9. Pittenger MF, Discher DE, Péault BM, Phinney DG, Hare JM, Caplan AI. Mesenchymal stem cell perspective: cell biology to clinical progress. Npj Regen Med. 2019;4:22.

10. Melchiorri AJ, Nguyen B-NB, Fisher JP. Mesenchymal Stem Cells: Roles and Relationships in Vascularization. Tissue Eng Part B Rev. 2014;20:218–28.

11. Di Somma M, Schaafsma W, Grillo E, Vliora M, Dakou E, Corsini M, et al. Natural Histogel-Based Bio-Scaffolds for Sustaining Angiogenesis in Beige Adipose Tissue. Cells. 2019;8:1457.

12. Alcayaga-Miranda F, Cuenca J, Khoury M. Antimicrobial Activity of Mesenchymal Stem Cells: Current Status and New Perspectives of Antimicrobial Peptide-Based Therapies. Front Immunol [Internet]. 2017 [cited 2020 Sep 9];8. Available from: http://journal.frontiersin.org/article/10.3389/fimmu.2017.00339/full

13. Bessède E, Dubus P, Mégraud F, Varon C. Helicobacter pylori infection and stem cells at the origin of gastric cancer. Oncogene. Nature Publishing Group; 2015;34:2547–55.

14. De Luca A, Gallo M, Aldinucci D, Ribatti D, Lamura L, D'Alessio A, et al. Role of the EGFR ligand/receptor system in the secretion of angiogenic factors in mesenchymal stem cells. J Cell Physiol. 2011;226:2131–8.

15. Ho J, Moyes DL, Tavassoli M, Naglik JR. The Role of ErbB Receptors in Infection. Trends Microbiol. 2017;25:942–52.

16. Krasnodembskaya A, Song Y, Fang X, Gupta N, Serikov V, Lee J-W, et al. Antibacterial Effect of Human Mesenchymal Stem Cells Is Mediated in Part from Secretion of the Antimicrobial Peptide LL-37. STEM CELLS. 2010;28:2229–38.

17. Meisel R, Brockers S, Heseler K, Degistirici Ö, Bülle H, Woite C, et al. Human but not murine multipotent mesenchymal stromal cells exhibit broad-spectrum antimicrobial effector function mediated by indoleamine 2,3-dioxygenase. Leukemia. 2011;25:648–54.

18. Gonzalez-Rey E, Anderson P, Gonzalez MA, Rico L, Buscher D, Delgado M. Human adult stem cells derived from adipose tissue protect against experimental colitis and sepsis. Gut. 2009;58:929–39.

19. Lee N-Y, Ko W-C, Hsueh P-R. Nanoparticles in the Treatment of Infections Caused by Multidrug-Resistant Organisms. Front Pharmacol [Internet]. Frontiers; 2019 [cited 2020 Oct 28];10. Available from: https://www.frontiersin.org/articles/10.3389/fphar.2019.01153/full

20. Sutton MT, Fletcher D, Ghosh SK, Weinberg A, van Heeckeren R, Kaur S, et al. Antimicrobial Properties of Mesenchymal Stem Cells: Therapeutic Potential for Cystic Fibrosis Infection, and Treatment. Stem Cells Int. 2016;2016:1–12.

21. Gupta N, Nizet V. Stabilization of Hypoxia-Inducible Factor-1 Alpha Augments the Therapeutic Capacity of Bone Marrow-Derived Mesenchymal Stem Cells in Experimental Pneumonia. Front Med. 2018;5:131.

22. Das B, Kashino SS, Pulu I, Kalita D, Swami V, Yeger H, et al. CD271+ Bone Marrow Mesenchymal Stem Cells May Provide a Niche for Dormant Mycobacterium tuberculosis. Sci Transl Med. 2013;5:170ra13-170ra13.

23. Fatima S, Kamble SS, Dwivedi VP, Bhattacharya D, Kumar S, Ranganathan A, et al. Mycobacterium tuberculosis programs mesenchymal stem cells to establish dormancy and persistence. J Clin Invest. 2019;130:655–61.

24. Scutera S, Salvi V, Lorenzi L, Piersigilli G, Lonardi S, Alotto D, et al. Adaptive Regulation of Osteopontin Production by Dendritic Cells Through the Bidirectional Interaction With Mesenchymal Stromal Cells. Front Immunol. 2018;9:1207.

25. Rezzola S, Di Somma M, Corsini M, Leali D, Ravelli C, Polli VAB, et al. VEGFR2 activation mediates the pro-angiogenic activity of BMP4. Angiogenesis. 2019;22:521–33.

26. Oviedo-Boyso J, Bravo-Patiño A, Baizabal-Aguirre VM. Collaborative Action of Toll-Like and Nod-Like Receptors as Modulators of the Inflammatory Response to Pathogenic Bacteria. Mediators Inflamm. 2014;2014:1–16.

27. McCord AM, Resto-Ruiz SI, Anderson BE. Autocrine Role for Interleukin-8 in Bartonella henselae-Induced Angiogenesis. Infect Immun. 2006;74:5185–90.

28. Rezaie J, Heidarzadeh M, Hassanpour M, Amini H, Shokrollahi E, Ahmadi M, et al. The Angiogenic Paracrine Potential of Mesenchymal Stem Cells. In: Ahmed Al-Anazi K, editor. Update Mesenchymal Induc Pluripotent Stem Cells [Internet]. IntechOpen; 2020 [cited 2020 Sep 10]. Available from: https://www.intechopen.com/books/update-on-mesenchymal-and-induced-pluripotent-stem-cells/the-angiogenic-paracrine-potential-of-mesenchymal-stem-cells

29. Nassiri SM, Rahbarghazi R. Interactions of Mesenchymal Stem Cells with Endothelial Cells. Stem Cells Dev. Mary Ann Liebert, Inc., publishers; 2013;23:319–32.

30. Dehio C. Bartonella –host-cell interactions and vascular tumour formation. Nat Rev Microbiol. Nature Publishing Group; 2005;3:621–31.

31. Vermi W. Role of dendritic cell-derived CXCL13 in the pathogenesis of Bartonella henselae B-rich granuloma. Blood. 2006;107:454–62.

32. Kempf VAJ, Schaller M, Behrendt S, Volkmann B, Aepfelbacher M, Cakman I, et al. Interaction of Bartonella henselae with endothelial cells results in rapid bacterial rRNA synthesis and replication. Cell Microbiol. 2000;2:431–41.

33. Kempf VAJ, Schairer A, Neumann D, Grassl GA, Lauber K, Lebiedziejewski M, et al. Bartonella henselae inhibits apoptosis in Mono Mac 6 cells: B. henselae inhibits apoptosis in monocytes. Cell Microbiol. 2004;7:91–104.

34. Truttmann MC, Misselwitz B, Huser S, Hardt W-D, Critchley DR, Dehio C. Bartonella henselae engages inside-out and outside-in signaling by integrin β1 and talin1 during invasome-mediated bacterial uptake. J Cell Sci. 2011;124:3591–602.

35. Najar M, Krayem M, Meuleman N, Bron D, Lagneaux L. Mesenchymal Stromal Cells and Toll-Like Receptor Priming: A Critical Review. Immune Netw. 2017;17:89.

36. Strober W, Murray PJ, Kitani A, Watanabe T. Signalling pathways and molecular interactions of NOD1 and NOD2. Nat Rev Immunol. 2006;6:9–20.

37. Haile PA, Votta BJ, Marquis RW, Bury MJ, Mehlmann JF, Singhaus R, et al. The Identification and Pharmacological Characterization of 6-(*tert* -Butylsulfonyl)- *N* -(5-fluoro-1 *H* -indazol-3-yl)quinolin-4-amine (GSK583), a Highly Potent and Selective Inhibitor of RIP2 Kinase. J Med Chem. 2016;59:4867–80.

38. Viala J, Chaput C, Boneca IG, Cardona A, Girardin SE, Moran AP, et al. Nod1 responds to peptidoglycan delivered by the Helicobacter pylori cag pathogenicity island. Nat Immunol. 2004;5:1166–74.

39. Kim JG, Lee SJ, Kagnoff MF. Nod1 Is an Essential Signal Transducer in Intestinal Epithelial Cells Infected with Bacteria That Avoid Recognition by Toll-Like Receptors. Infect Immun. 2004;72:1487–95.

40. Opitz B, Förster S, Hocke AC, Maass M, Schmeck B, Hippenstiel S, et al. Nod1-Mediated Endothelial Cell Activation by *Chlamydophila pneumoniae*. Circ Res. 2005;96:319–26.

41. Tigno-Aranjuez JT, Asara JM, Abbott DW. Inhibition of RIP2's tyrosine kinase activity limits NOD2-driven cytokine responses. Genes Dev. 2010;24:2666–77.

42. Duran A, Valero N, Mosquera J, Fuenmayor E, Alvarez-Mon M. Gefitinib and pyrrolidine dithiocarbamate decrease viral replication and cytokine production in dengue virus infected human monocyte cultures. Life Sci. 2017;191:180–5.

43. Bentz GL, Yurochko AD. Human CMV infection of endothelial cells induces an angiogenic response through viral binding to EGF receptor and β1 and β3 integrins. Proc Natl Acad Sci. National Academy of Sciences; 2008;105:5531–6.

44. Singh B, Carpenter G, Coffey RJ. EGF receptor ligands: recent advances. F1000Research. 2016;5:2270.

45. Swanson KV, Griffiss JM, Edwards VL, Stein DC, Song W. Neisseria gonorrhoeae-induced transactivation of EGFR enhances gonococcal invasion. Cell Microbiol. 2011;13:1078–90.

584 46. Keates S, Keates AC, Katchar K, Peek, Jr. RM, Kelly CP. *Helicobacter pylori* Induces
585 Up- Regulation of the Epidermal Growth Factor Receptor in AGS Gastric Epithelial Cells. J Infect
586 Dis. 2007;196:95–103.

587 47. Zhang J, Li H, Wang J, Dong Z, Mian S, Yu F-SX. Role of EGFR Transactivation in Preventing
588 Apoptosis in Pseudomonas aeruginosa–Infected Human Corneal Epithelial Cells. Invest
589 Ophthalmol Vis Sci. 2004;45:2569–76.

590 48. Yan F, Cao H, Chaturvedi R, Krishna U, Hobbs SS, Dempsey PJ, et al. Epidermal growth factor
591 receptor activation protects gastric epithelial cells from Helicobacter pylori-induced apoptosis.
592 Gastroenterology. 2009;136:1297–307, e1-3.

593 49. Brandau S, Jakob M, Bruderek K, Bootz F, Giebel B, Radtke S, et al. Mesenchymal Stem Cells
594 Augment the Anti-Bacterial Activity of Neutrophil Granulocytes. PLOS ONE. Public Library of
595 Science; 2014;9:e106903.

596 50. Chandra PK, Gerlach SL, Wu C, Khurana N, Swientoniewski LT, Abdel-Mageed AB, et al.
597 Mesenchymal stem cells are attracted to latent HIV-1-infected cells and enable virus reactivation
598 via a non-canonical PI3K-NFκB signaling pathway. Sci Rep. 2018;8:14702.

599 51. Del Prete A, Scutera S, Sozzani S, Musso T. Role of osteopontin in dendritic cell shaping of
600 immune responses. Cytokine Growth Factor Rev. 2019;50:19–28.

601 52. Raghuvanshi S, Sharma P, Singh S, Van Kaer L, Das G. Mycobacterium tuberculosis evades
602 host immunity by recruiting mesenchymal stem cells. Proc Natl Acad Sci. 2010;107:21653–8.

603 53. Dehghani Nazhvani A, Ahzan S, Hosseini S-M, Attar A, Monabati A, Tavangar MS.
604 Purification of Stem Cells from Oral Pyogenic Granuloma Tissue. Open Dent J. 2018;12:560–6.

605 54. Mitroulis I, Kalafati L, Bornhäuser M, Hajishengallis G, Chavakis T. Regulation of the Bone
606 Marrow Niche by Inflammation. Front Immunol [Internet]. Frontiers; 2020 [cited 2020 Nov 19];11.
607 Available from: https://www.frontiersin.org/articles/10.3389/fimmu.2020.01540/full

608 55. Perucca S, Di Palma A, Piccaluga PP, Gemelli C, Zoratti E, Bassi G, et al. Mesenchymal
609 stromal cells (MSCs) induce ex vivo proliferation and erythroid commitment of cord blood
610 haematopoietic stem cells (CB-CD34+ cells). PloS One. 2017;12:e0172430.

611 56. Hipp SJ, O??Shields A, Fordham LA, Blatt J, Hamrick HJ, Henderson FW. Multifocal Bone
612 Marrow Involvement in Cat-Scratch Disease: Pediatr Infect Dis J. 2005;24:472–4.

613 57. Donà D, Nai Fovino L, Mozzo E, Cabrelle G, Bordin G, Lundin R, et al. Osteomyelitis in Cat-
614 Scratch Disease: A Never-Ending Dilemma—A Case Report and Literature Review. Case Rep
615 Pediatr. 2018;2018:1–8.

616 58. Randell MG, Balakrishnan N, Gunn- Christie R, Mackin A, Breitschwerdt EB. Bartonella
617 henselae infection in a dog with recalcitrant ineffective erythropoiesis. Vet Clin Pathol.
618 2018;47:45–50.

619

620

621

Ethics Statement

This study was carried out in accordance with the recommendations of "Comitato Etico Interaziendale A.O.U. Città della Salute e della Scienza di Torino—A.O. Ordine Mauriziano—ASL TO1, number 0009806" with written informed consent from all subjects. All subjects gave written informed consent in accordance with the Declaration of Helsinki. The protocol was approved by the "Comitato Etico Interaziendale A.O.U. Città della Salute e della Scienza di Torino—A.O. Ordine Mauriziano—ASL TO1."

Availability of data and materials

All data and materials are available upon request.

Author Contributions

SaS, SM, SiS, and TM participated in the design of the study.

SaS, RS, GP, EG, MB, VS, DA, and TS participated in data acquisition and analysis.

TM, SM and SaS wrote the manuscript.

SiS participated in data interpretation and manuscript revision.

Conflict of Interest Statement

The authors declare that the research was conducted in the absence of any commercial or financial relationships that could be construed as a potential conflict of interest.

Acknowledgments

The authors thank Prof William Vermi, Department of Molecular and Translational Medicine, University of Brescia, for immunohistochemistry analysis of the MSC/*B. henselae* interaction.

Funding

This work was supported by funds from the Compagnia di San Paolo, Fondazione Ricerca Molinette, AIRC (Associazione Italiana Ricerca sul Cancro) project IG15811 (2015–2017) and project IG 20776 (2017).

FIGURE LEGENDS

FIG 1. ***B. henselae*** **invades and persists in MSCs.** (A) Invasion rates of *B. henselae* into MSCs were measured at day 1, 2, 3, 4 and 8 pi by gentamicin protection assay (GPA). After infection, cells were treated with gentamicin, and the number of intracellular bacteria was determined by CFU count. Data are expressed as means ± SEM from two independent experiments carried out in triplicate (*$P < 0.05$ *vs* Log_{10} CFU at 1 d; unpaired t-test). (B) Uninfected (CTRL) or *B. henselae*-infected MSCs (8 days) were immunostained with an anti-*BH* antibody and counterstained with hematoxylin (upper panel 20X, lower panel 40X). (C) To determine intracellular survival after 4 days of infection, extracellular bacteria were killed by gentamicin treatment and incubated in normal medium for the indicated times. Mean values ± SEM of triplicate samples are representative of three independent experiments. (*$P < 0.05$; unpaired t-test). (D) Invasion rates of *B. henselae* in MSCs or HUVECs (60,000 cells each, respectively). The number of intracellular bacteria as Log_{10} CFU was quantified at 1 day pi (*$P < 0.05$ MSCs *vs* HUVECs; unpaired t-test).

FIG 2. ***B. henselae*** **localizes in invasome structures in MSCs**. (A) Immunofluorescence of *B. henselae*-infected MSCs at 1, 2, 4 and 8 days pi and uninfected control MSCs (CTLR). *B. henselae* and cell membranes were stained with DAPI (cyan) and wheat germ agglutinin-Alexa Fluor 594 (red), respectively, and analyzed with an epifluorescence microscope. Bacteria anchored to the MSC membrane are indicated with arrowheads. The thin arrows (2 and 4 days) indicate internalized bacteria within membrane bound compartments in the perinuclear area, whereas the large arrows (8 days) highlight sizeable intracellular bacterial aggregates called invasomes. Each image also shows the basal portion of adherent MSC cells, with the orthogonal z reconstruction of the whole cell. **(B)** Representative image of an invasome. MSCs were infected with *B. henselae* for 8 days and then

672 washed and fixed with PFA. Samples were stained for F-actin (red), wheat germ agglutinin (WGA)
673 (green) and DAPI and analyzed as described in panel A (bar: 10 µm).

674 **FIG 3. *B. henselae* favors the proliferation of infected MSCs.** (A) MSC death was evaluated by
675 FACS analysis after 4 days of infection with *B. henselae.* Uninfected MSCs (left panel; CTRL) and
676 infected MSCs (right panel; *B. henselae*) were double-stained with FITC-annexin V and PI.
677 Counterstaining with PI allowed differentiation of necrotic cells (upper left quadrant of the dot
678 plot), late apoptotic cells (upper right quadrant) and early apoptotic cells (lower right quadrant). The
679 percentages of cells localizing to these quadrants are indicated in each quadrant. Data are
680 representative of 3independent experiments. (B) The Bcl-2/Bax expression ratio was analyzed in
681 control and *B. henselae*-infected MSCs at 2 days pi by qPCR. Gene expression was normalized to
682 HPRT. Data are expressed as means ± SEM of 4 independent experiments (ns not significant;
683 unpaired t-test). (C) Proliferation assay. MSCs were treated as indicated for 0, 2, 4, and 8 days and
684 analyzed by MTT assay. Untreated MSCs (white circle); *B. henselae* infected MSC (black circle);
685 and heat killed *B. henselae*-treated MSCs (HKB.h.) (grey circle). Data are expressed as means ±
686 SEM of triplicate samples of one experiment representative of 3 independent ones (*$P < 0.05$ *B.*
687 *henselae vs* CTRL, unpaired t-test).

688 **FIG 4. Expression of TLR2, NOD1 and EGFR in *B. henselae*-infected MSCs**. (A) mRNA
689 expression levels of TLR2, TLR4, NOD1 and EGFR in uninfected (white bar) and *B. henselae*-
690 infected MSCs (black bar) were determined by qPCR and normalized to RPL13A. Data are
691 expressed as means ± SEM of four independent experiments (* $P < 0.05$; unpaired t-test). (B) TLR2
692 and TLR4 protein expression levels on MSC membranes were analyzed by FACS in MSCs at 4 d
693 pi. Cells were immunostained with anti-TLR2, anti-TLR4 or specific isotype control antibodies.
694 The percentages of positive cells are indicated in each quadrant. Fluorescence minus one (FMO)
695 controls for the antibodies are shown as well. Data are representative of three independent
696 experiments. (C) Cell extracts from MSCs infected with *B. henselae* for 30, 60, and 120 min or with

hEGF (50 ng/mL) for 15 min were subjected to immunoblotting using anti-EGFR pY1068 or anti-EGFR antibodies. (D) Analysis of CXCL8 in the supernatants from uninfected or *B. henselae*-infected MSCs pre-treated or not for 6 h with a neutralizing anti-TLR2 antibody (10 μg/mL) or with the EGFR inhibitor gefitinib (10 μM) or the RIP2K inhibitor GSK583 (1 μM) and then stimulated for 96 h. Data are shown as percentage (Mean ± SEM) of CXCL8 production compared to DMSO or specific isotype control antibody-treated cells set at 100% (n=6 for antiTLR2; n=4 for gefitinib, n=3 for GSK583; * $P < 0.05$ *vs B. henselae*-infected cells; unpaired t-test). (E) To evaluate *B. henselae* internalization, MSC were pretreated for 6 h with the neutralizing anti-EGFR (10 μg/mL) or gefitinib (10 μM), and percentages of intracellular bacteria were determined, after 1 and 2 days of incubation, respect to DMSO or specific isotype control antibody-treated cells set at 100%. Data are shown as mean ± SEM (n=4 for gefitinib, n=2 for EGFR experiments performed in duplicate; * $P < 0.05$ *vs* internalized bacteria in untreated cells; unpaired t-test).

FIG 5. Conditioned medium from *B. henselae*-infected MSCs curbs the infection rates and angiogenic response of HUVECs. The effects of conditioned medium (CM) from *B. henselae*-infected MSCs were tested by means of different angiogenic assays. (A) HUVEC monolayers were wounded with a 1.0-mm-wide rubber policeman and incubated in fresh medium supplemented with 5% FCS and 1:2 diluted CM from infected (black bar, CM-MSC CTRL) or uninfected (white bar, CM-MSC *B. henselae*) MSCs. After 1 day, HUVECs invading the wound were quantified by digital imaging. Mean ± SEM of 4 measurements *per* sample. *$P < 0.05$ *vs* Ctrl; unpaired t-test. (B) Sprouting analysis of HUVEC spheroids. Spheroids were prepared in 20% methylcellulose medium, embedded in fibrin gel and stimulated with 1:2 diluted CM obtained from MSCs treated in the presence (black bar) or absence (white bar) of bacteria or with 30 ng/ml VEGF-A (dashed bar). The number of growing cell sprouts was counted after 1 day. Data are expressed as mean ± SEM (n=10-20) and indicated as fold increase in the number of sprouts/spheroid *vs* Ctrl. *$P < 0.05$*vs* Ctrl; unpaired t-test. (C) The effect of CM from uninfected *vs B. henselae*-infected MSCs on HUVEC

morphogenesis was assessed by tube morphogenesis assay in three-dimensional (3D) collagen matrix. HUVECs were seeded (40000 cells/cm^2) on Cultrex Extracellular Matrix in the presence of 1:2 diluted CM from uninfected (white bar) or *B. henselae*-infected MSCs (black bar). After 8 h, the formation of capillary-like structures was examined. Representative images are shown in the left panels. The quantifications of capillary-like structure (right panel) are expressed as means ± SEM relative to three measurements *per* sample. * $P < 0.05$ *vs* Ctrl; unpaired t-test. (D) Invasion rate of *B. henselae* in HUVECs (expressed as total CFUs) after 1 day of infection in the absence (grey bar) or presence of 1:2 diluted CM-MSC CTRL (white bar) and CM-MSC *B. henselae* (black bar). * $P <$ 0.05; unpaired t-test.

FIG 6. Angiogenic signature of *B. henselae*-infected MSCs. (A) Human angiogenesis antibody array analysis was performed using a pool of supernatants from 96 h uninfected MSC (CTRL) or *B. henselae*-infected MSCs. Some of the most representative angiogenic factors are highlighted in different colors. The graph with normalized pixel density of all the visualized spots is shown in Fig. S1 in the supplemental material. (B) Heat map analysis representing the normalized average pixel density of the pair of duplicate spots for each angiogenic-related protein in the array. (C) Quantification of VEGF-A, CXCL8, IL-6, CCL5 and PDGF-D production in uninfected (CTRL) and *B. henselae*-infected MSCs. Data are expressed as mean ± SEM of 3 independent experiments. * P < 0.05 *vs* CTRL; unpaired t-test. nd= not detectable.

743 **Figure 1**

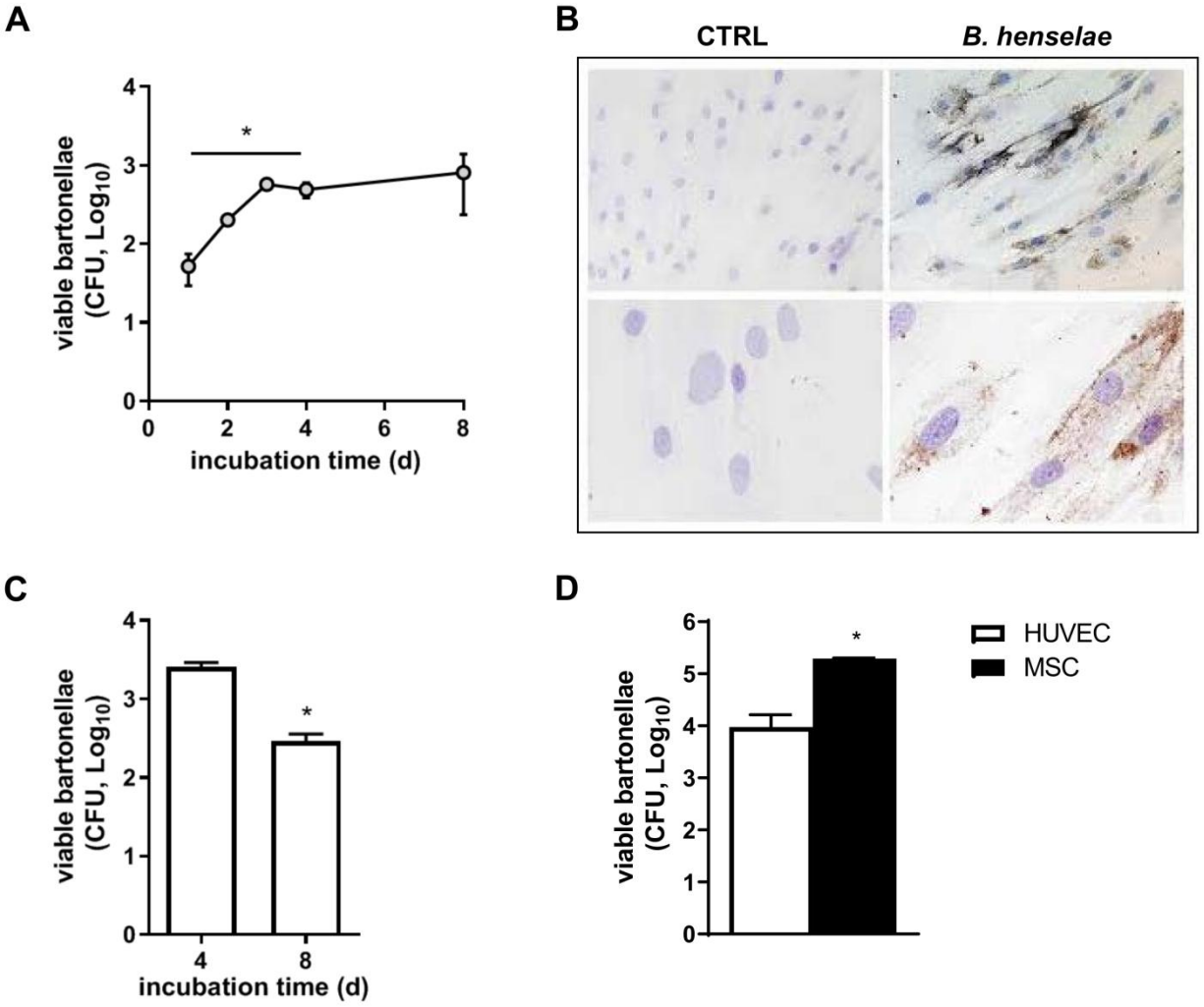

744

745

746

747

748

749

750

751

752

753

754

755

756

757 **Figure 2**

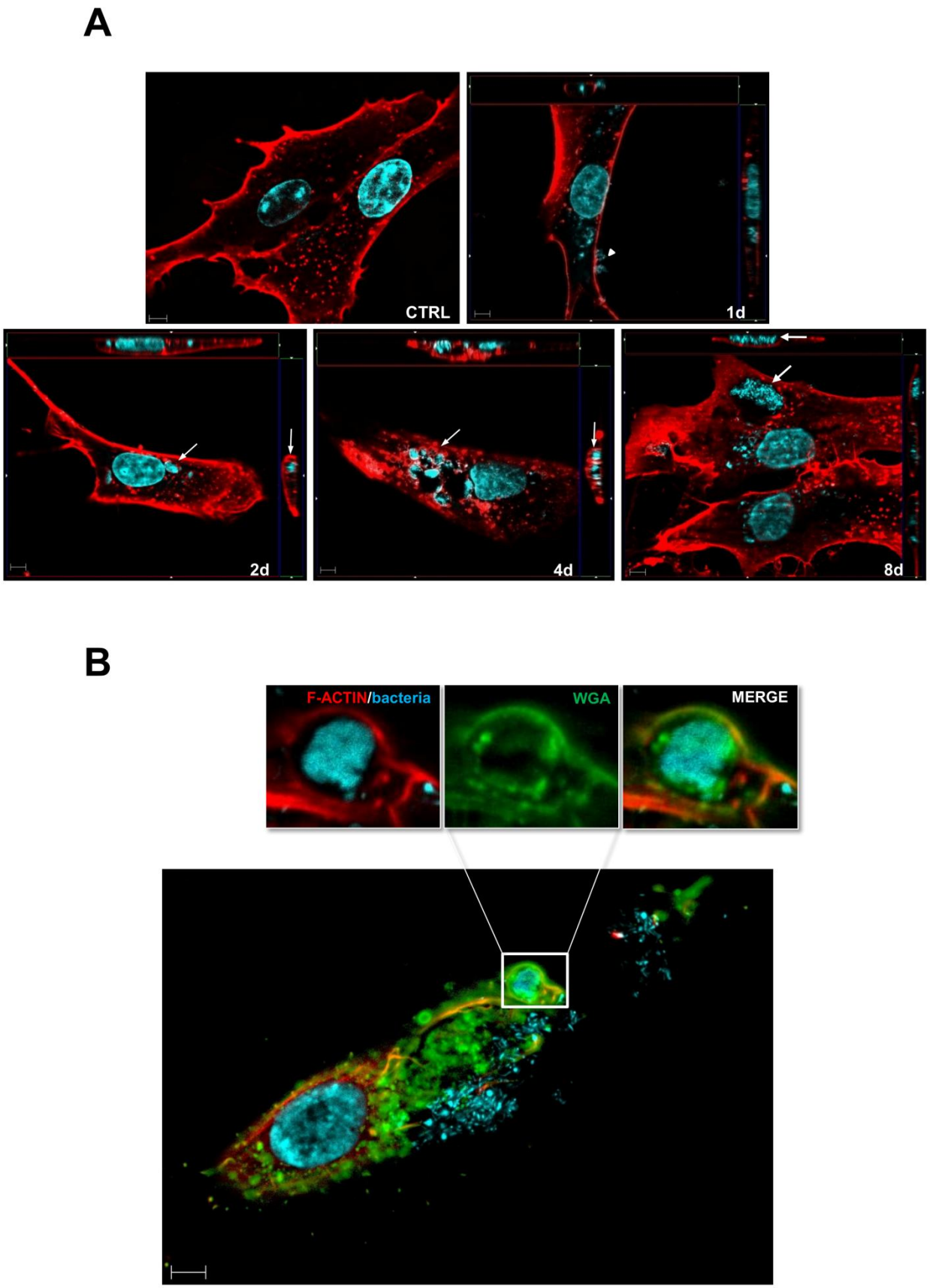

758

Figure 3

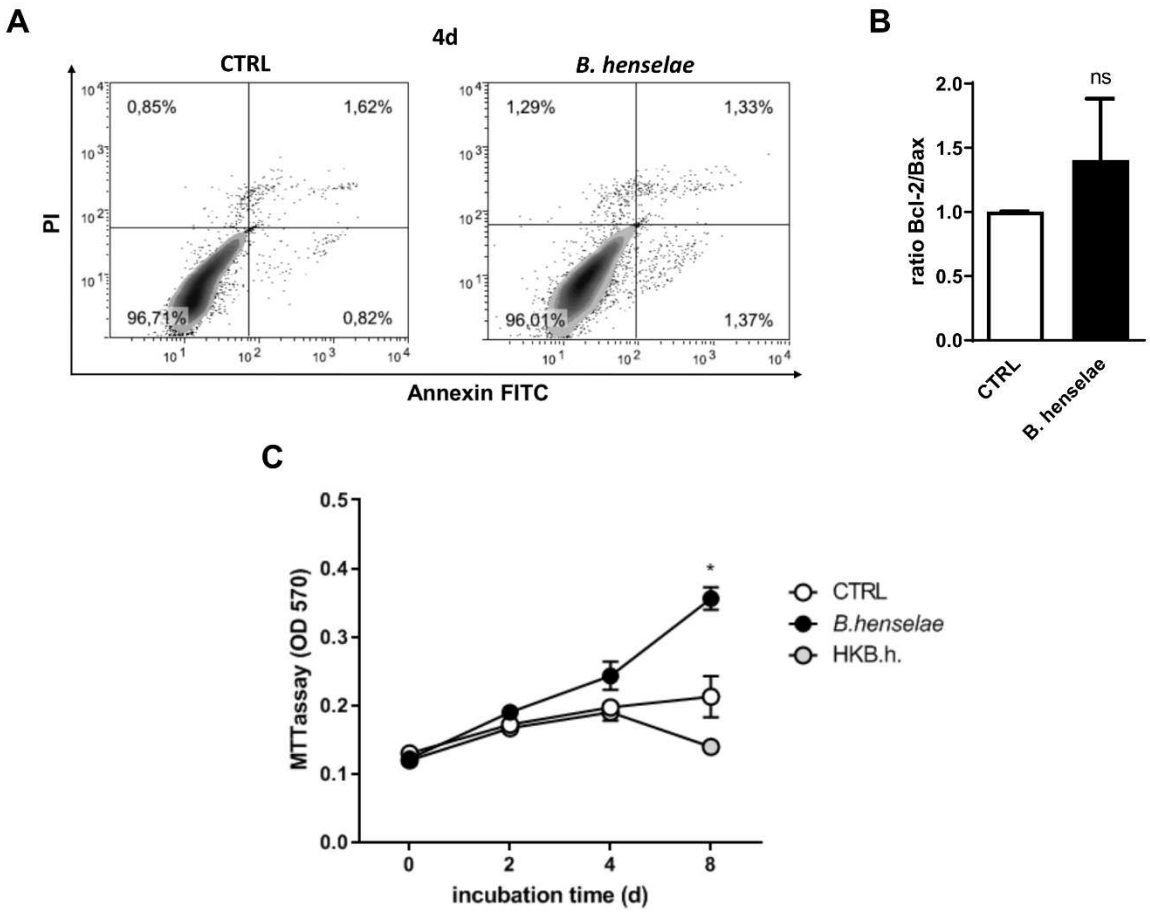
A
4d
CTRL
B. henselae
0,85%
1,62%
96,71%
0,82%
1,29%
1,33%
96,01%
1,37%
PI
Annexin FITC
B
ns
ratio Bcl-2/Bax
CTRL
B. henselae
C
MTTassay (OD 570)
incubation time (d)
CTRL
B.henselae
HKB.h.

Figure 4

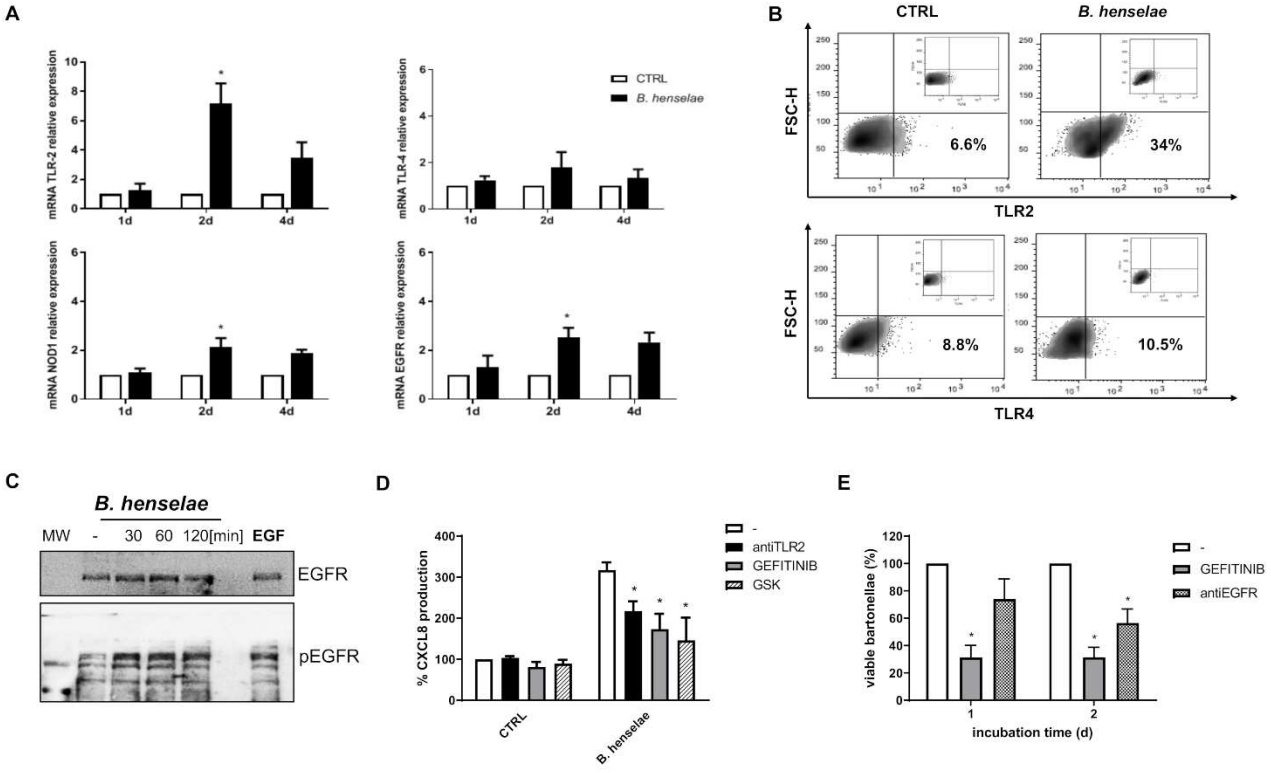
A
mRNA TLR-2 relative expression
mRNA TLR-4 relative expression
mRNA NOD1 relative expression
mRNA EGFR relative expression
1d
2d
4d
CTRL
B. henselae
B
CTRL
B. henselae
FSC-H
6.6%
34%
TLR2
8.8%
10.5%
TLR4
C
B. henselae
MW - 30 60 120[min] EGF
EGFR
pEGFR
D
% CXCL8 production
antiTLR2
GEFITINIB
GSK
CTRL
B. henselae
E
viable bartonellae (%)
GEFITINIB
antiEGFR
incubation time (d)

Figure 5

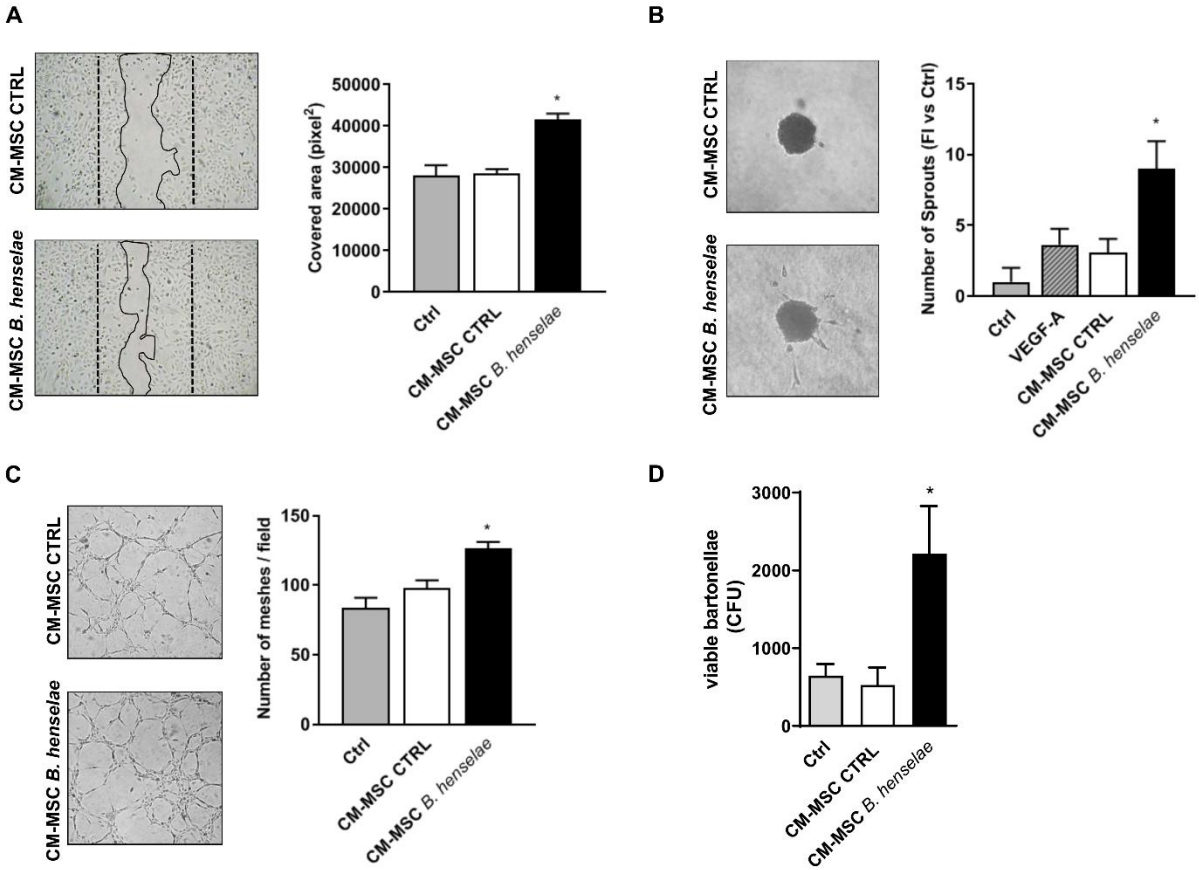
A
CM-MSC CTRL
CM-MSC B. henselae
Covered area (pixel²)
50000
40000
30000
20000
10000
0
*
Ctrl
CM-MSC CTRL
CM-MSC B. henselae
B
CM-MSC CTRL
CM-MSC B. henselae
Number of Sprouts (FI vs Ctrl)
15
10
5
0
*
Ctrl
VEGF-A
CM-MSC CTRL
CM-MSC B. henselae
C
CM-MSC CTRL
CM-MSC B. henselae
Number of meshes / field
150
100
50
0
*
Ctrl
CM-MSC CTRL
CM-MSC B. henselae
D
viable bartonellae (CFU)
3000
2000
1000
0
*
Ctrl
CM-MSC CTRL
CM-MSC B. henselae

Figure 6

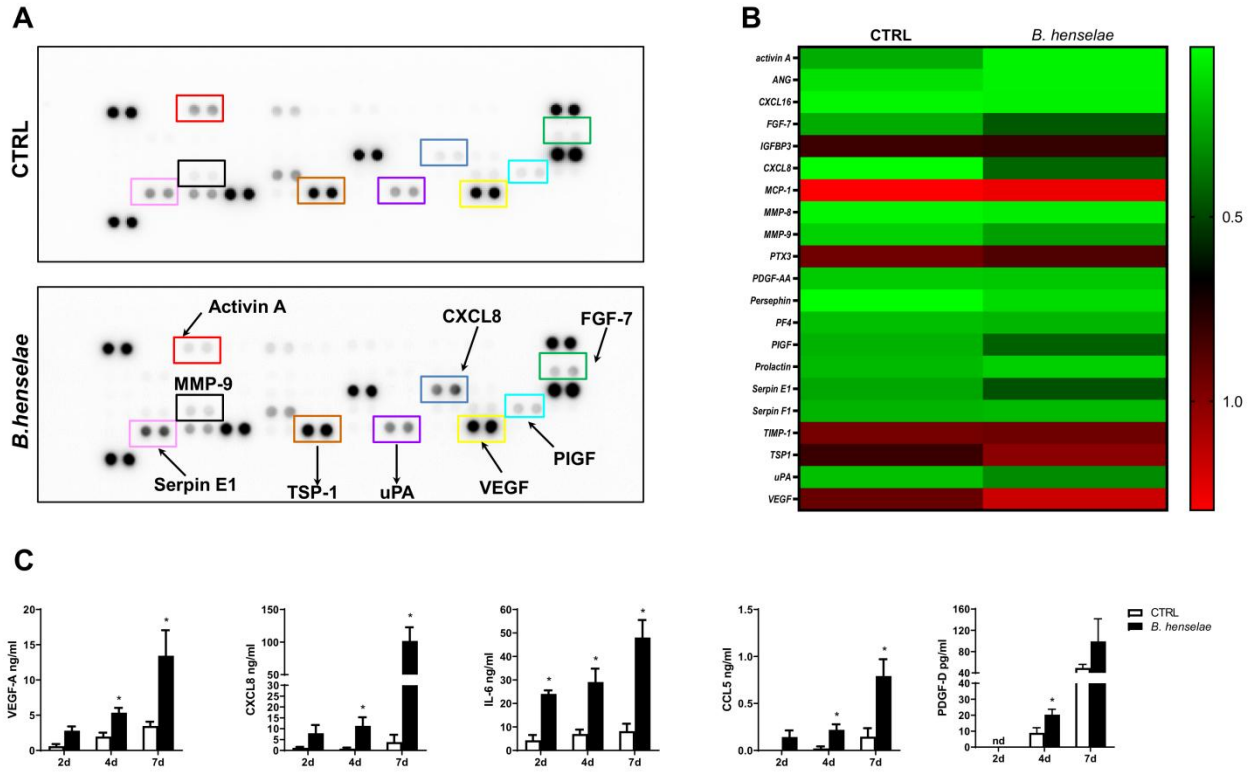
A
CTRL
B.henselae
Activin A
MMP-9
Serpin E1
TSP-1
uPA
CXCL8
VEGF
FGF-7
PIGF
B
CTRL
B. henselae
activin A
ANG
CXCL16
FGF-7
IGFBP3
CXCL8
MCP-1
MMP-8
MMP-9
PTX3
PDGF-AA
Persephin
PF4
PlGF
Prolactin
Serpin E1
Serpin F1
TIMP-1
TSP1
uPA
VEGF
0.5
1.0
C
VEGF-A ng/ml
CXCL8 ng/ml
IL-6 ng/ml
CCL5 ng/ml
PDGF-D pg/ml
nd
2d
4d
7d
CTRL
B. henselae

Figures

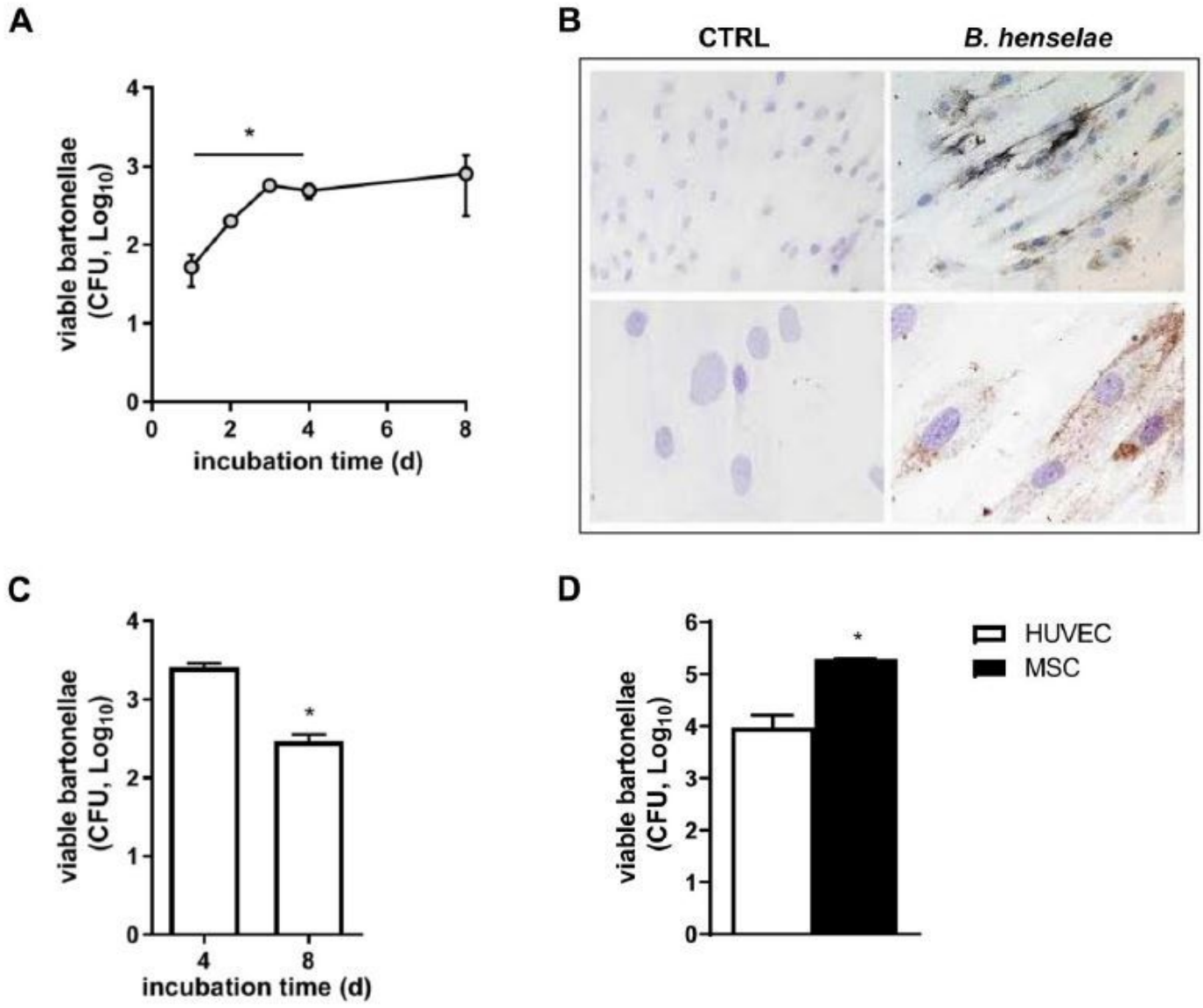

Figure 1

B. henselae invades and persists in MSCs. (A) Invasion rates of B. henselae into MSCs were measured at day 1, 2, 3, 4 and 8 pi by gentamicin protection assay (GPA). After infection, cells were treated with gentamicin, and the number of intracellular bacteria was determined by CFU count. Data are expressed as means ± SEM from two independent experiments carried out in triplicate (*P < 0.05 vs Log10 CFU at 1 d; unpaired t-test). (B) Uninfected (CTRL) or B. henselae- infected MSCs (8 days) were immunostained with an anti-BH antibody and counterstained with hematoxylin (upper panel 20X, lower panel 40X). (C) To determine intracellular survival after 4 days of infection, extracellular bacteria were killed by gentamicin treatment and incubated in normal medium for the indicated times. Mean values ± SEM of triplicate samples are representative of three independent experiments. (*P < 0.05; unpaired t-test). (D) Invasion

rates of B. henselae in MSCs or HUVECs (60,000 cells each, respectively). The number of intracellular bacteria as Log10 CFU was quantified at 1 day pi (*P < 0.05 MSCs vs HUVECs; unpaired t-test).

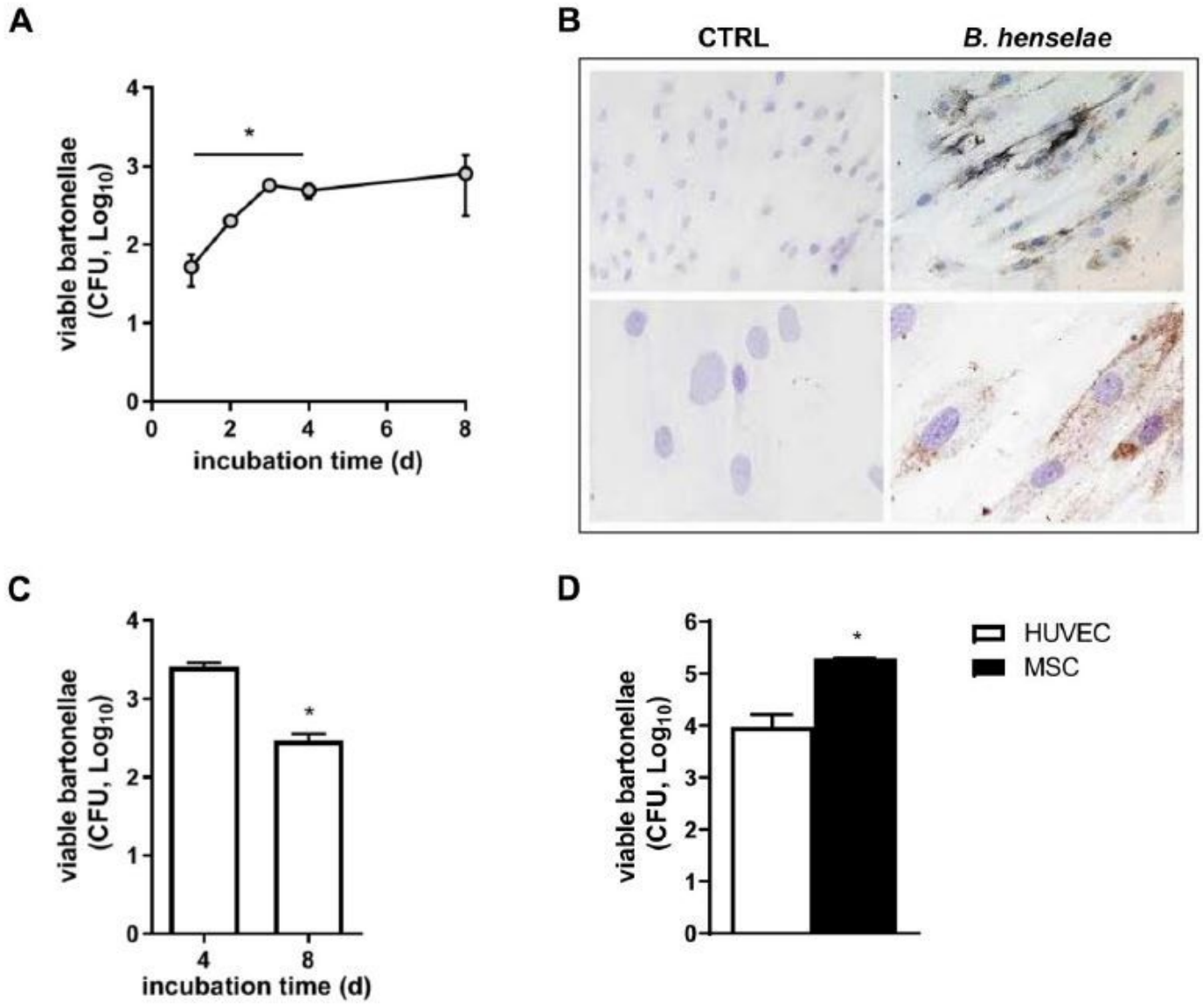

Figure 1

B. henselae invades and persists in MSCs. (A) Invasion rates of B. henselae into MSCs were measured at day 1, 2, 3, 4 and 8 pi by gentamicin protection assay (GPA). After infection, cells were treated with gentamicin, and the number of intracellular bacteria was determined by CFU count. Data are expressed as means ± SEM from two independent experiments carried out in triplicate (*P < 0.05 vs Log10 CFU at 1 d; unpaired t-test). (B) Uninfected (CTRL) or B. henselae- infected MSCs (8 days) were immunostained with an anti-BH antibody and counterstained with hematoxylin (upper panel 20X, lower panel 40X). (C) To determine intracellular survival after 4 days of infection, extracellular bacteria were killed by gentamicin treatment and incubated in normal medium for the indicated times. Mean values ± SEM of triplicate samples are representative of three independent experiments. (*P < 0.05; unpaired t-test). (D) Invasion

rates of B. henselae in MSCs or HUVECs (60,000 cells each, respectively). The number of intracellular bacteria as Log10 CFU was quantified at 1 day pi (*P < 0.05 MSCs vs HUVECs; unpaired t-test).

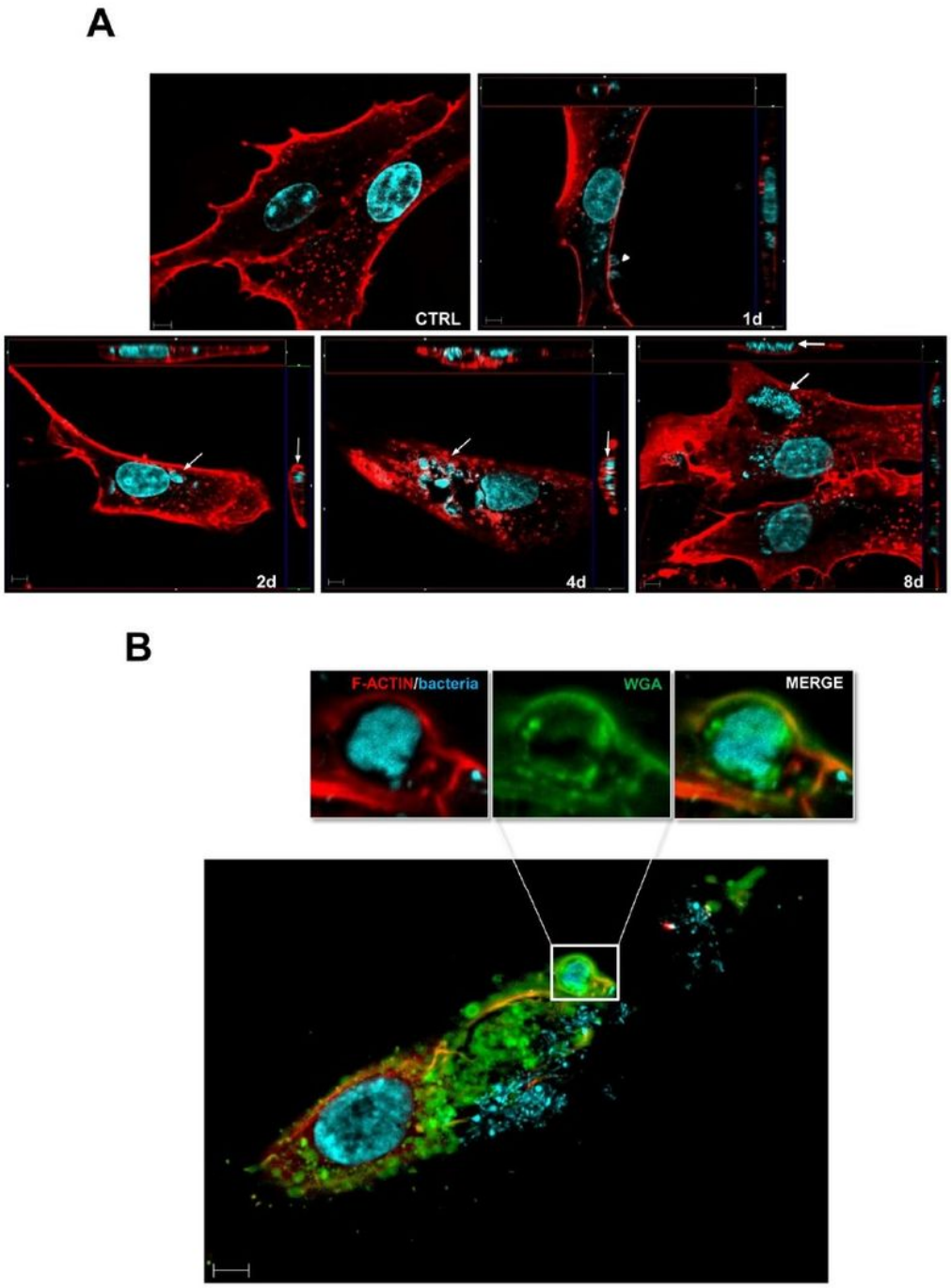

Figure 2

B. henselae localizes in invasome structures in MSCs. (A) Immunofluorescence of B. henselae-infected MSCs at 1, 2, 4 and 8 days pi and uninfected control MSCs (CTLR). B. henselae and cell membranes were stained with DAPI (cyan) and wheat germ agglutinin-Alexa Fluor 594 (red), respectively, and analyzed

with an epifluorescence microscope. Bacteria anchored to the MSC membrane are indicated with arrowheads. The thin arrows (2 and 4 days) indicate internalized bacteria within membrane bound compartments in the perinuclear area, whereas the large arrows (8 days) highlight sizeable intracellular bacterial aggregates called invasomes. Each image also shows the basal portion of adherent MSC cells, with the orthogonal z reconstruction of the whole cell. (B) Representative image of an invasome. MSCs were infected with B. henselae for 8 days and then washed and fixed with PFA. Samples were stained for F-actin (red), wheat germ agglutinin (WGA) (green) and DAPI and analyzed as described in panel A (bar: 10 μm).

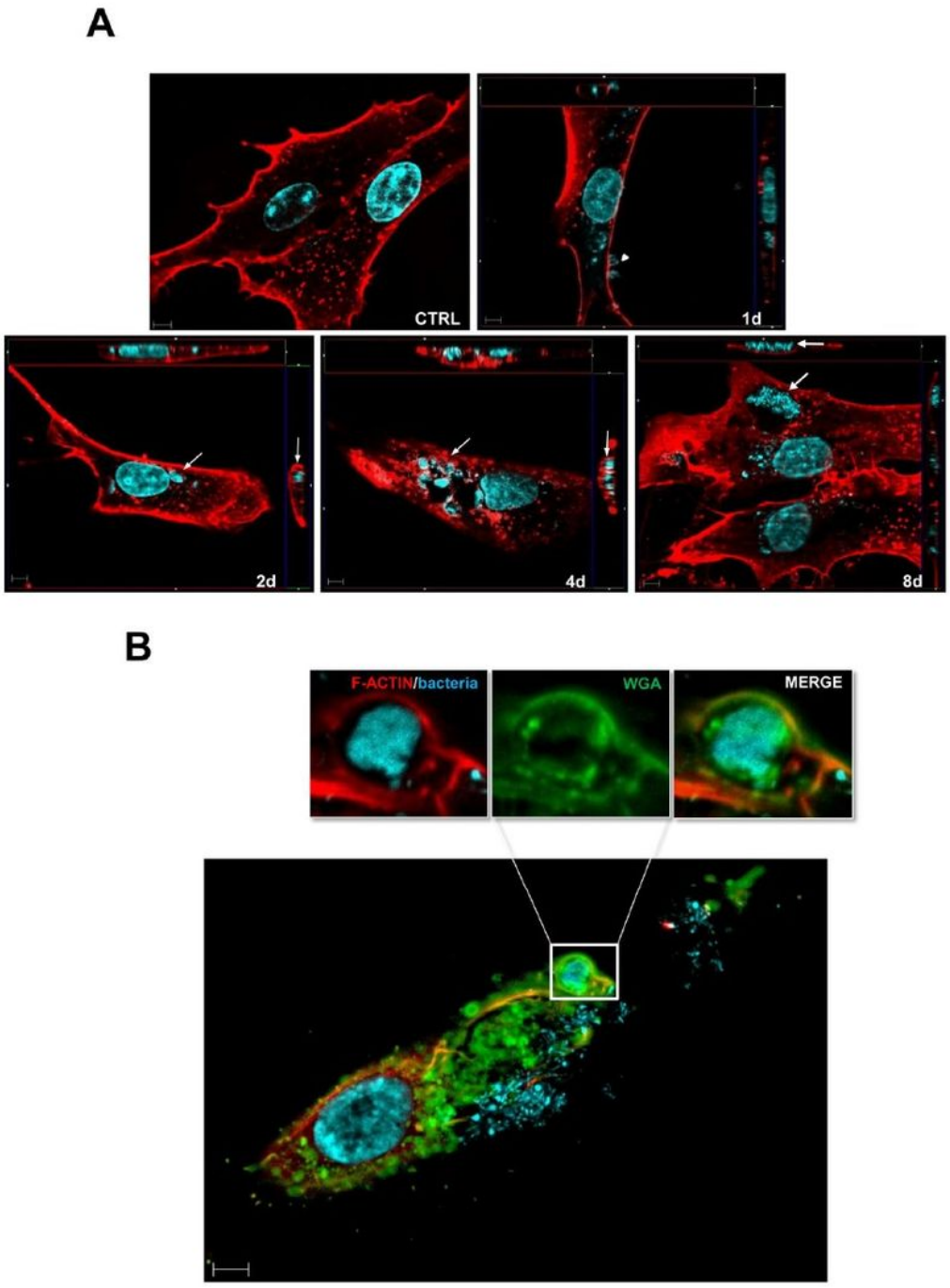

Figure 2

B. henselae localizes in invasome structures in MSCs. (A) Immunofluorescence of B. henselae-infected MSCs at 1, 2, 4 and 8 days pi and uninfected control MSCs (CTLR). B. henselae and cell membranes were stained with DAPI (cyan) and wheat germ agglutinin-Alexa Fluor 594 (red), respectively, and analyzed with an epifluorescence microscope. Bacteria anchored to the MSC membrane are indicated with arrowheads. The thin arrows (2 and 4 days) indicate internalized bacteria within membrane bound

compartments in the perinuclear area, whereas the large arrows (8 days) highlight sizeable intracellular bacterial aggregates called invasomes. Each image also shows the basal portion of adherent MSC cells, with the orthogonal z reconstruction of the whole cell. (B) Representative image of an invasome. MSCs were infected with B. henselae for 8 days and then washed and fixed with PFA. Samples were stained for F-actin (red), wheat germ agglutinin (WGA) (green) and DAPI and analyzed as described in panel A (bar: 10 µm).

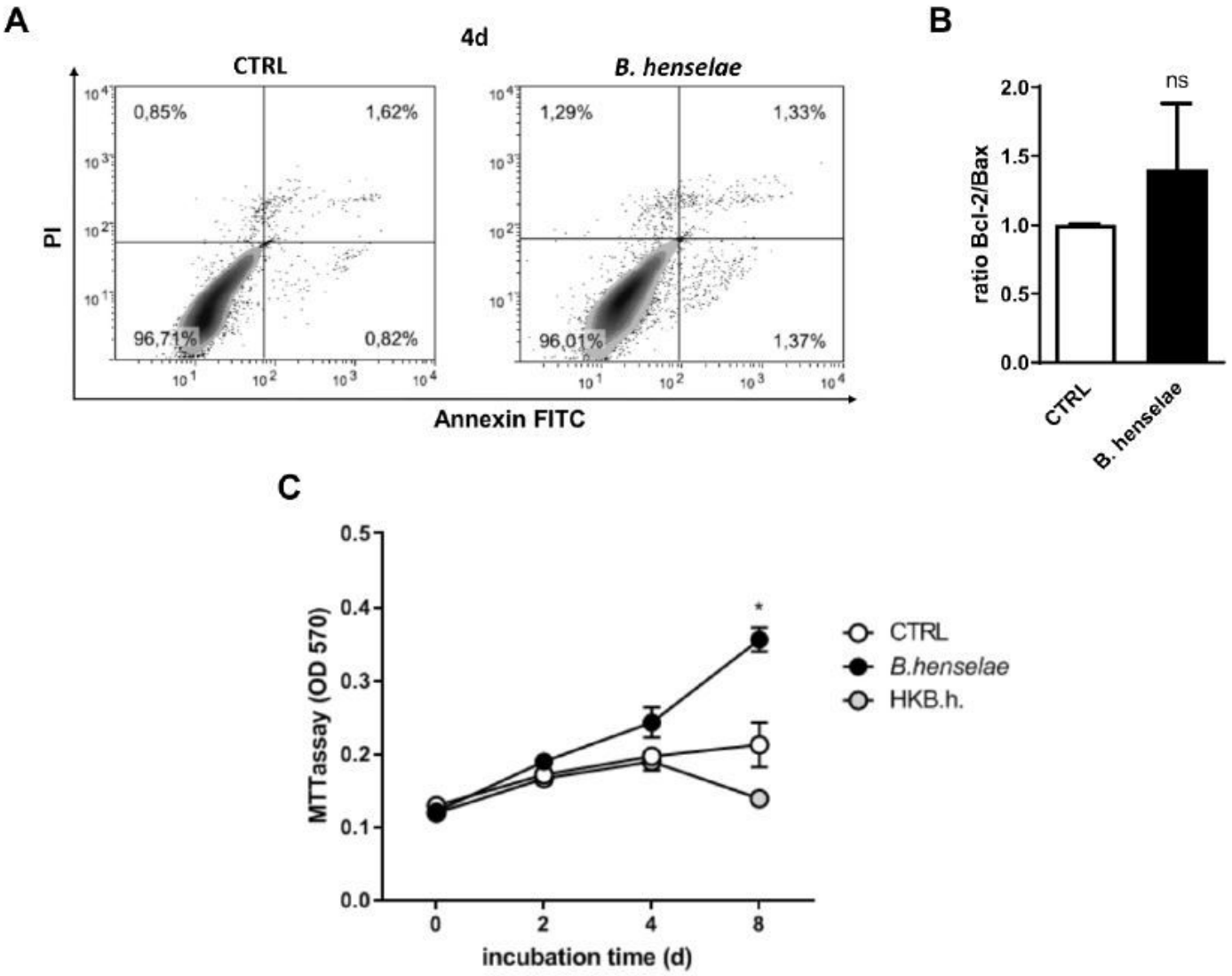

Figure 3

B. henselae favors the proliferation of infected MSCs. (A) MSC death was evaluated by FACS analysis after 4 days of infection with B. henselae. Uninfected MSCs (left panel; CTRL) and infected MSCs (right panel; B. henselae) were double-stained with FITC-annexin V and PI. Counterstaining with PI allowed differentiation of necrotic cells (upper left quadrant of the dot plot), late apoptotic cells (upper right quadrant) and early apoptotic cells (lower right quadrant). The percentages of cells localizing to these quadrants are indicated in each quadrant. Data are representative of 3independent experiments. (B) The

Bcl-2/Bax expression ratio was analyzed in control and B. henselae-infected MSCs at 2 days pi by qPCR. Gene expression was normalized to HPRT. Data are expressed as means ± SEM of 4 independent experiments (ns not significant; unpaired t-test). (C) Proliferation assay. MSCs were treated as indicated for 0, 2, 4, and 8 days and analyzed by MTT assay. Untreated MSCs (white circle); B. henselae infected MSC (black circle); and heat killed B. henselae-treated MSCs (HKB.h.) (grey circle). Data are expressed as means ± SEM of triplicate samples of one experiment representative of 3 independent ones (*P < 0.05 B. henselae vs CTRL, unpaired t-test).

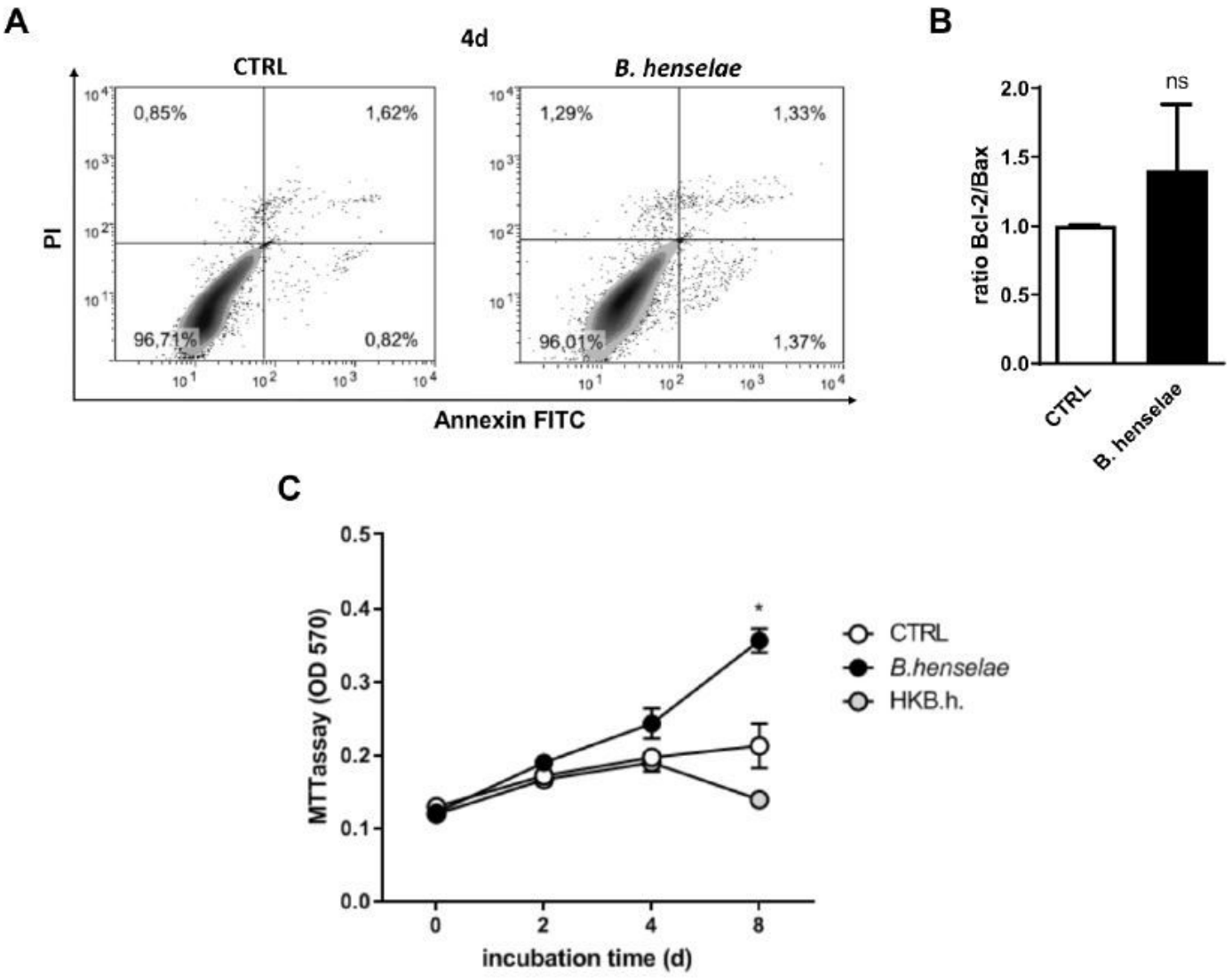

Figure 3

B. henselae favors the proliferation of infected MSCs. (A) MSC death was evaluated by FACS analysis after 4 days of infection with B. henselae. Uninfected MSCs (left panel; CTRL) and infected MSCs (right panel; B. henselae) were double-stained with FITC-annexin V and PI. Counterstaining with PI allowed differentiation of necrotic cells (upper left quadrant of the dot plot), late apoptotic cells (upper right quadrant) and early apoptotic cells (lower right quadrant). The percentages of cells localizing to these

quadrants are indicated in each quadrant. Data are representative of 3independent experiments. (B) The Bcl-2/Bax expression ratio was analyzed in control and B. henselae-infected MSCs at 2 days pi by qPCR. Gene expression was normalized to HPRT. Data are expressed as means ± SEM of 4 independent experiments (ns not significant; unpaired t-test). (C) Proliferation assay. MSCs were treated as indicated for 0, 2, 4, and 8 days and analyzed by MTT assay. Untreated MSCs (white circle); B. henselae infected MSC (black circle); and heat killed B. henselae-treated MSCs (HKB.h.) (grey circle). Data are expressed as means ± SEM of triplicate samples of one experiment representative of 3 independent ones (*P < 0.05 B. henselae vs CTRL, unpaired t-test).

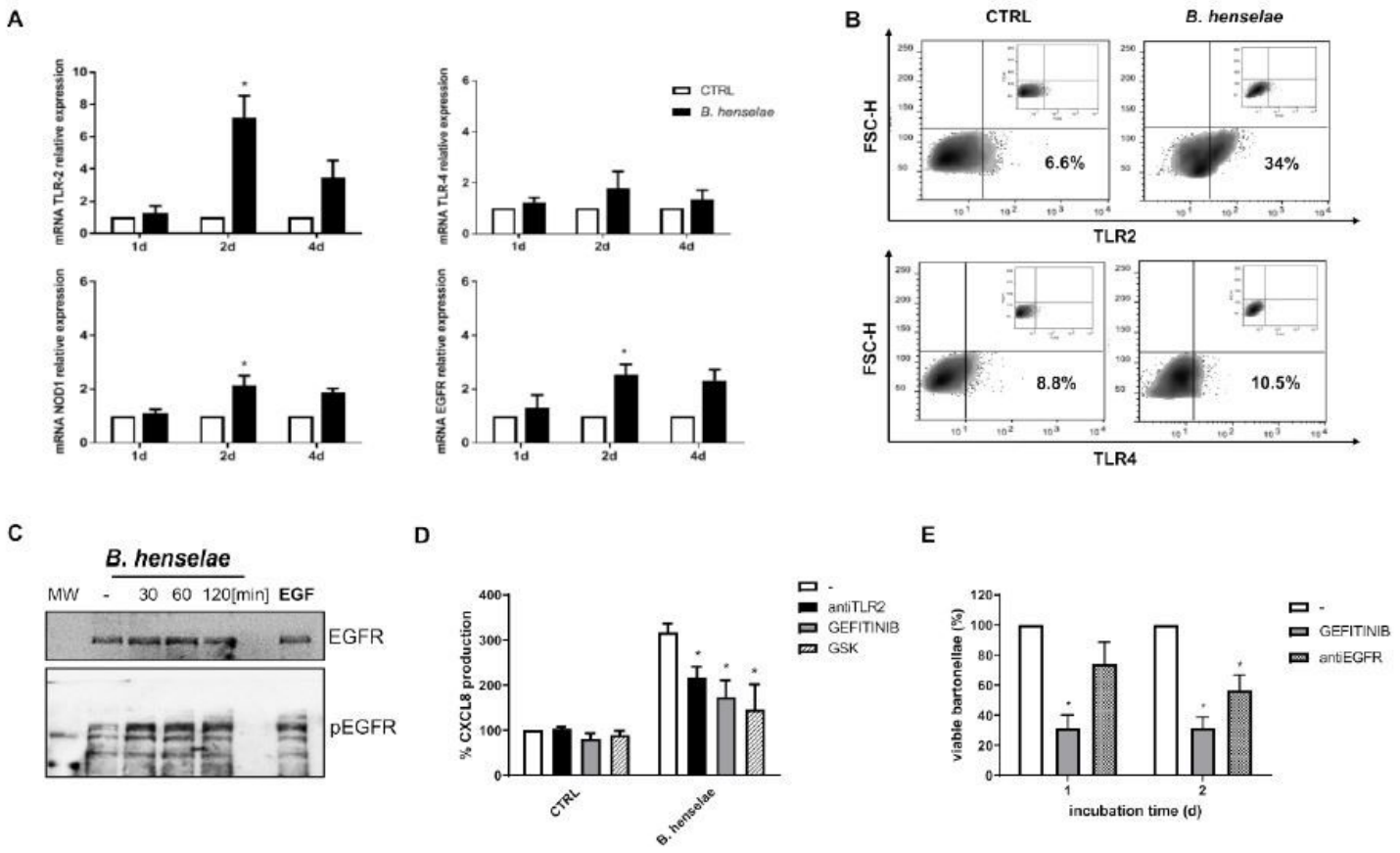

Figure 4

Expression of TLR2, NOD1 and EGFR in B. henselae-infected MSCs. (A) mRNA expression levels of TLR2, TLR4, NOD1 and EGFR in uninfected (white bar) and B. henselae-infected MSCs (black bar) were determined by qPCR and normalized to RPL13A. Data are expressed as means ± SEM of four independent experiments (* P < 0.05; unpaired t-test). (B) TLR2 and TLR4 protein expression levels on MSC membranes were analyzed by FACS in MSCs at 4 d pi. Cells were immunostained with anti-TLR2, anti-TLR4 or specific isotype control antibodies. The percentages of positive cells are indicated in each quadrant. Fluorescence minus one (FMO) controls for the antibodies are shown as well. Data are representative of three independent experiments. (C) Cell extracts from MSCs infected with B. henselae for 30, 60, and 120 min or with hEGF (50 ng/mL) for 15 min were subjected to immunoblotting using anti-EGFR pY1068 or anti-EGFR antibodies. (D) Analysis of CXCL8 in the supernatants from uninfected or B.

henselae-infected MSCs pre-treated or not for 6 h with a neutralizing anti-TLR2 antibody (10 µg/mL) or with the EGFR inhibitor gefitinib (10 µM) or the RIP2K inhibitor GSK583 (1 µM) and then stimulated for 96 h. Data are shown as percentage (Mean ± SEM) of CXCL8 production compared to DMSO or specific isotype control antibody-treated cells set at 100% (n=6 for antiTLR2; n=4 for gefitinib, n=3 for GSK583; * P < 0.05 vs B. henselae-infected cells; unpaired t-test). (E) To evaluate B. henselae internalization, MSC were pretreated for 6 h with the neutralizing anti-EGFR (10 µg/mL) or gefitinib (10 µM), and percentages of intracellular bacteria were determined, after 1 and 2 days of incubation, respect to DMSO or specific isotype control antibody-treated cells set at 100%. Data are shown as mean ± SEM (n=4 for gefitinib, n=2 for EGFR experiments performed in duplicate; *P < 0.05 vs internalized bacteria in untreated cells; unpaired t-test).

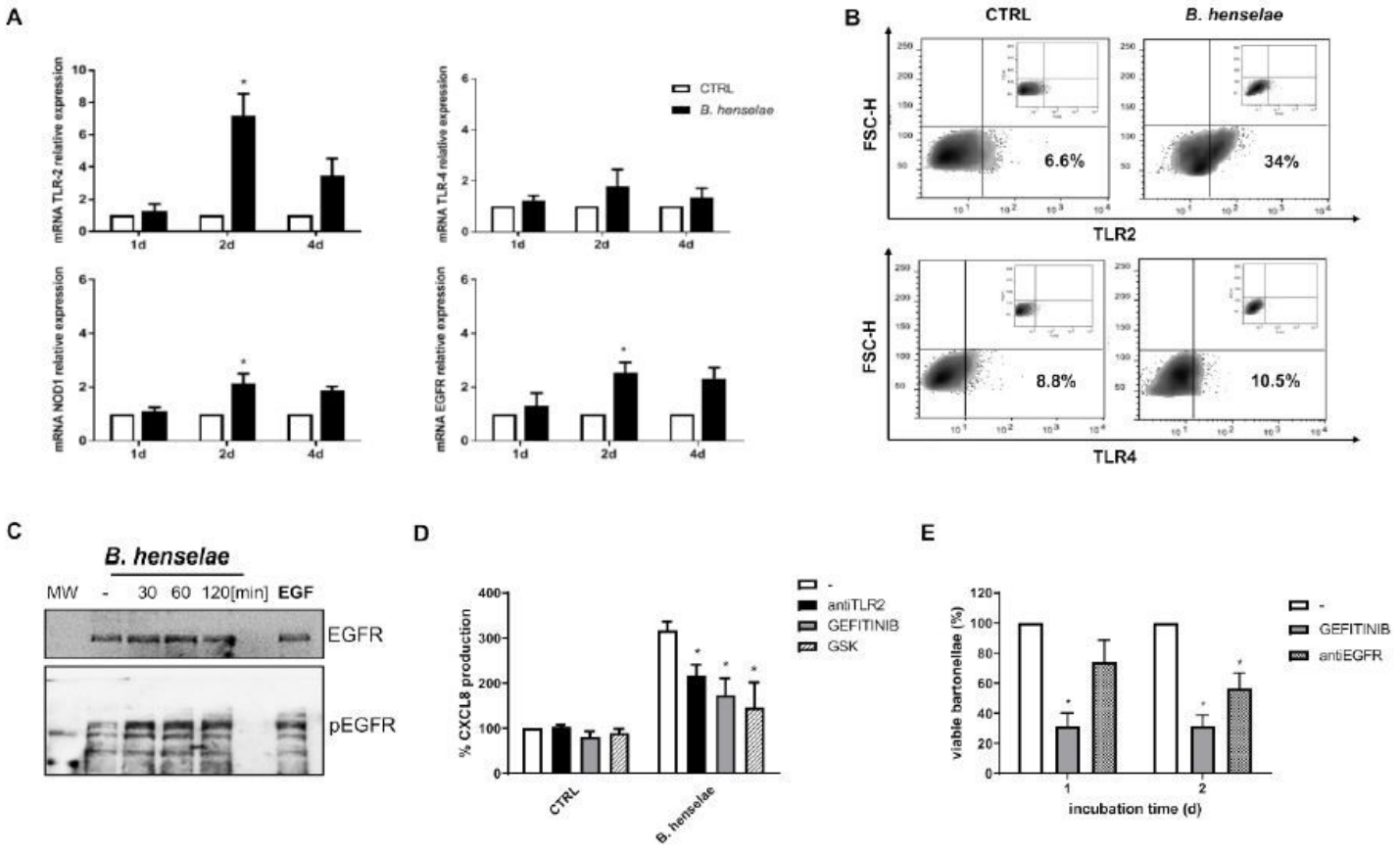

Figure 4

Expression of TLR2, NOD1 and EGFR in B. henselae-infected MSCs. (A) mRNA expression levels of TLR2, TLR4, NOD1 and EGFR in uninfected (white bar) and B. henselae-infected MSCs (black bar) were determined by qPCR and normalized to RPL13A. Data are expressed as means ± SEM of four independent experiments (* P < 0.05; unpaired t-test). (B) TLR2 and TLR4 protein expression levels on MSC membranes were analyzed by FACS in MSCs at 4 d pi. Cells were immunostained with anti-TLR2, anti-TLR4 or specific isotype control antibodies. The percentages of positive cells are indicated in each quadrant. Fluorescence minus one (FMO) controls for the antibodies are shown as well. Data are representative of three independent experiments. (C) Cell extracts from MSCs infected with B. henselae

for 30, 60, and 120 min or with hEGF (50 ng/mL) for 15 min were subjected to immunoblotting using anti-EGFR pY1068 or anti-EGFR antibodies. (D) Analysis of CXCL8 in the supernatants from uninfected or B. henselae-infected MSCs pre-treated or not for 6 h with a neutralizing anti-TLR2 antibody (10 µg/mL) or with the EGFR inhibitor gefitinib (10 µM) or the RIP2K inhibitor GSK583 (1 µM) and then stimulated for 96 h. Data are shown as percentage (Mean ± SEM) of CXCL8 production compared to DMSO or specific isotype control antibody-treated cells set at 100% (n=6 for antiTLR2; n=4 for gefitinib, n=3 for GSK583; * P < 0.05 vs B. henselae-infected cells; unpaired t-test). (E) To evaluate B. henselae internalization, MSC were pretreated for 6 h with the neutralizing anti-EGFR (10 µg/mL) or gefitinib (10 µM), and percentages of intracellular bacteria were determined, after 1 and 2 days of incubation, respect to DMSO or specific isotype control antibody-treated cells set at 100%. Data are shown as mean ± SEM (n=4 for gefitinib, n=2 for EGFR experiments performed in duplicate; *P < 0.05 vs internalized bacteria in untreated cells; unpaired t-test).

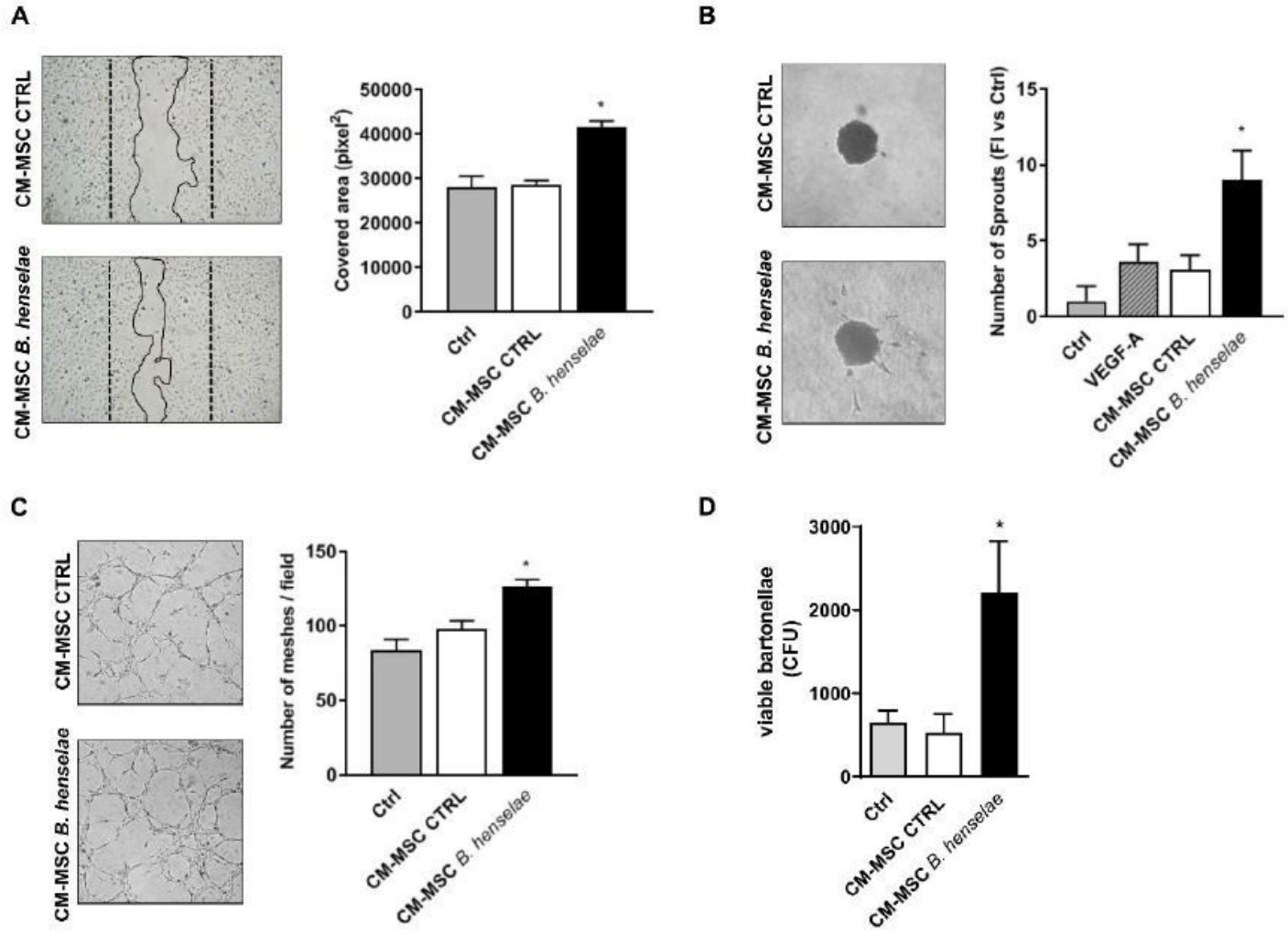

Figure 5

Conditioned medium from B. henselae-infected MSCs curbs the infection rates and angiogenic response of HUVECs. The effects of conditioned medium (CM) from B. henselae-infected MSCs were tested by means of different angiogenic assays. (A) HUVEC monolayers were wounded with a 1.0-mm-wide rubber

policeman and incubated in fresh medium supplemented with 5% FCS and 1:2 diluted CM from infected (black bar, CM-MSC CTRL) or uninfected (white bar, CM-MSC B. henselae) MSCs. After 1 day, HUVECs invading the wound were quantified by digital imaging. Mean ± SEM of 4 measurements per sample. *P < 0.05 vs Ctrl; unpaired t-test. (B) Sprouting analysis of HUVEC spheroids. Spheroids were prepared in 20% methylcellulose medium, embedded in fibrin gel and stimulated with 1:2 diluted CM obtained from MSCs treated in the presence (black bar) or absence (white bar) of bacteria or with 30 ng/ml VEGF-A (dashed bar). The number of growing cell sprouts was counted after 1 day. Data are expressed as mean ± SEM (n=10-20) and indicated as fold increase in the number of sprouts/spheroid vs Ctrl. *P < 0.05vs Ctrl; unpaired t-test. (C) The effect of CM from uninfected vs B. henselae-infected MSCs on HUVEC morphogenesis was assessed by tube morphogenesis assay in three-dimensional (3D) collagen matrix. HUVECs were seeded (40000 cells/cm2) on Cultrex Extracellular Matrix in the presence of 1:2 diluted CM from uninfected (white bar) or B. henselae-infected MSCs (black bar). After 8 h, the formation of capillary-like structures was examined. Representative images are shown in the left panels. The quantifications of capillary-like structure (right panel) are expressed as means ± SEM relative to three measurements per sample. * P < 0.05 vs Ctrl; unpaired t-test. (D) Invasion rate of B. henselae in HUVECs (expressed as total CFUs) after 1 day of infection in the absence (grey bar) or presence of 1:2 diluted CM-MSC CTRL (white bar) and CM-MSC B. henselae (black bar). * P < 0.05; unpaired t-test.

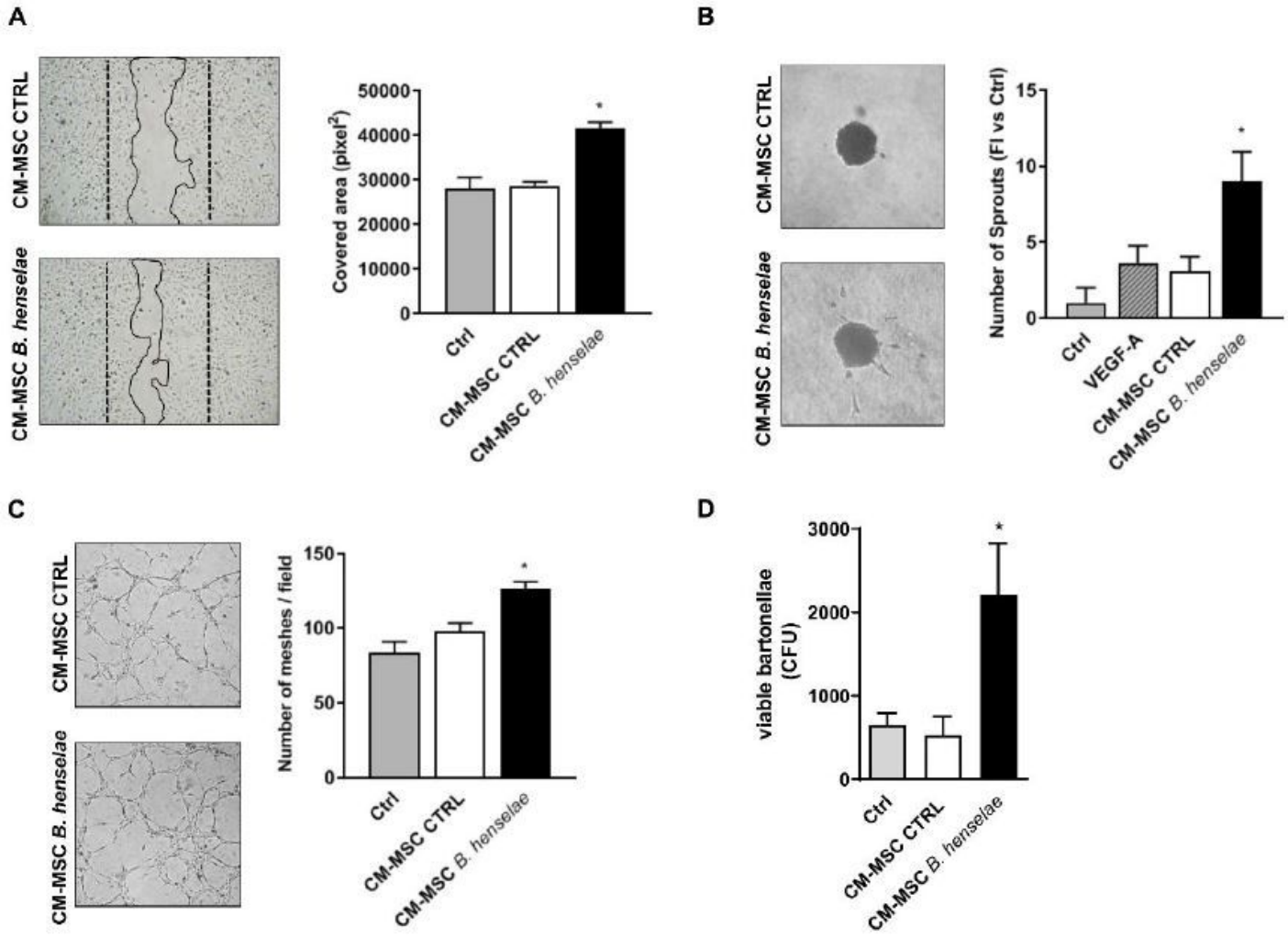

Figure 5

Conditioned medium from B. henselae-infected MSCs curbs the infection rates and angiogenic response of HUVECs. The effects of conditioned medium (CM) from B. henselae-infected MSCs were tested by means of different angiogenic assays. (A) HUVEC monolayers were wounded with a 1.0-mm-wide rubber policeman and incubated in fresh medium supplemented with 5% FCS and 1:2 diluted CM from infected (black bar, CM-MSC CTRL) or uninfected (white bar, CM-MSC B. henselae) MSCs. After 1 day, HUVECs invading the wound were quantified by digital imaging. Mean ± SEM of 4 measurements per sample. *P < 0.05 vs Ctrl; unpaired t-test. (B) Sprouting analysis of HUVEC spheroids. Spheroids were prepared in 20% methylcellulose medium, embedded in fibrin gel and stimulated with 1:2 diluted CM obtained from MSCs treated in the presence (black bar) or absence (white bar) of bacteria or with 30 ng/ml VEGF-A (dashed bar). The number of growing cell sprouts was counted after 1 day. Data are expressed as mean ± SEM (n=10-20) and indicated as fold increase in the number of sprouts/spheroid vs Ctrl. *P < 0.05vs Ctrl; unpaired t-test. (C) The effect of CM from uninfected vs B. henselae-infected MSCs on HUVEC morphogenesis was assessed by tube morphogenesis assay in three-dimensional (3D) collagen matrix. HUVECs were seeded (40000 cells/cm2) on Cultrex Extracellular Matrix in the presence of 1:2 diluted CM from uninfected (white bar) or B. henselae-infected MSCs (black bar). After 8 h, the formation of capillary-like structures was examined. Representative images are shown in the left panels. The quantifications of capillary-like structure (right panel) are expressed as means ± SEM relative to three measurements per sample. * P < 0.05 vs Ctrl; unpaired t-test. (D) Invasion rate of B. henselae in HUVECs (expressed as total CFUs) after 1 day of infection in the absence (grey bar) or presence of 1:2 diluted CM-MSC CTRL (white bar) and CM-MSC B. henselae (black bar). * P < 0.05; unpaired t-test.

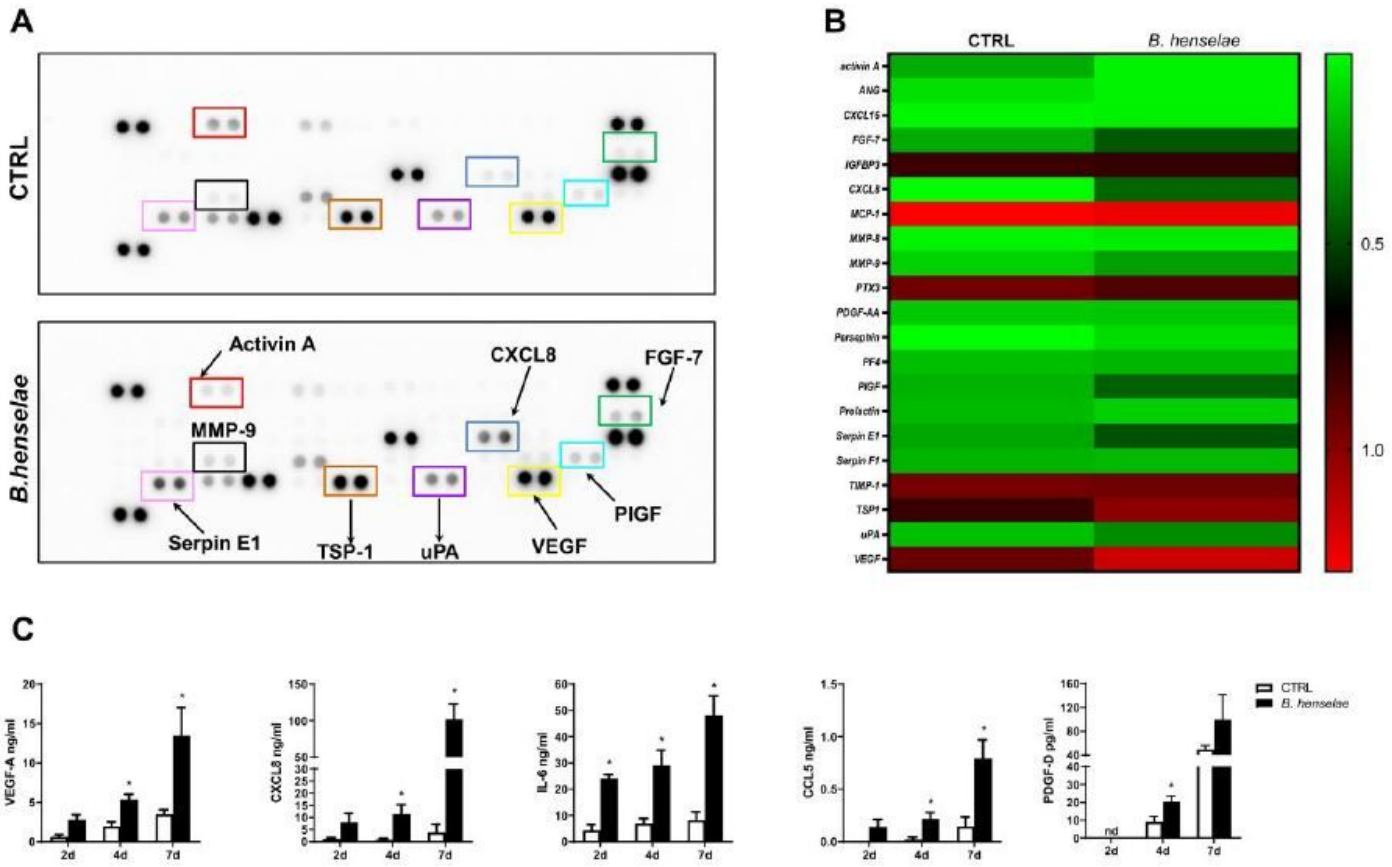

Figure 6

Angiogenic signature of B. henselae-infected MSCs. (A) Human angiogenesis antibody array analysis was performed using a pool of supernatants from 96 h uninfected MSC (CTRL) or B. henselae-infected MSCs. Some of the most representative angiogenic factors are highlighted in different colors. The graph with normalized pixel density of all the visualized spots is shown in Fig. S1 in the supplemental material. (B) Heat map analysis representing the normalized average pixel density of the pair of duplicate spots for each angiogenic-related protein in the array. (C) Quantification of VEGF-A, CXCL8, IL-6, CCL5 and PDGF-D production in uninfected (CTRL) and B. henselae-infected MSCs. Data are expressed as mean ± SEM of 3 independent experiments. * $P < 0.05$ vs CTRL; unpaired t-test. nd= not detectable.

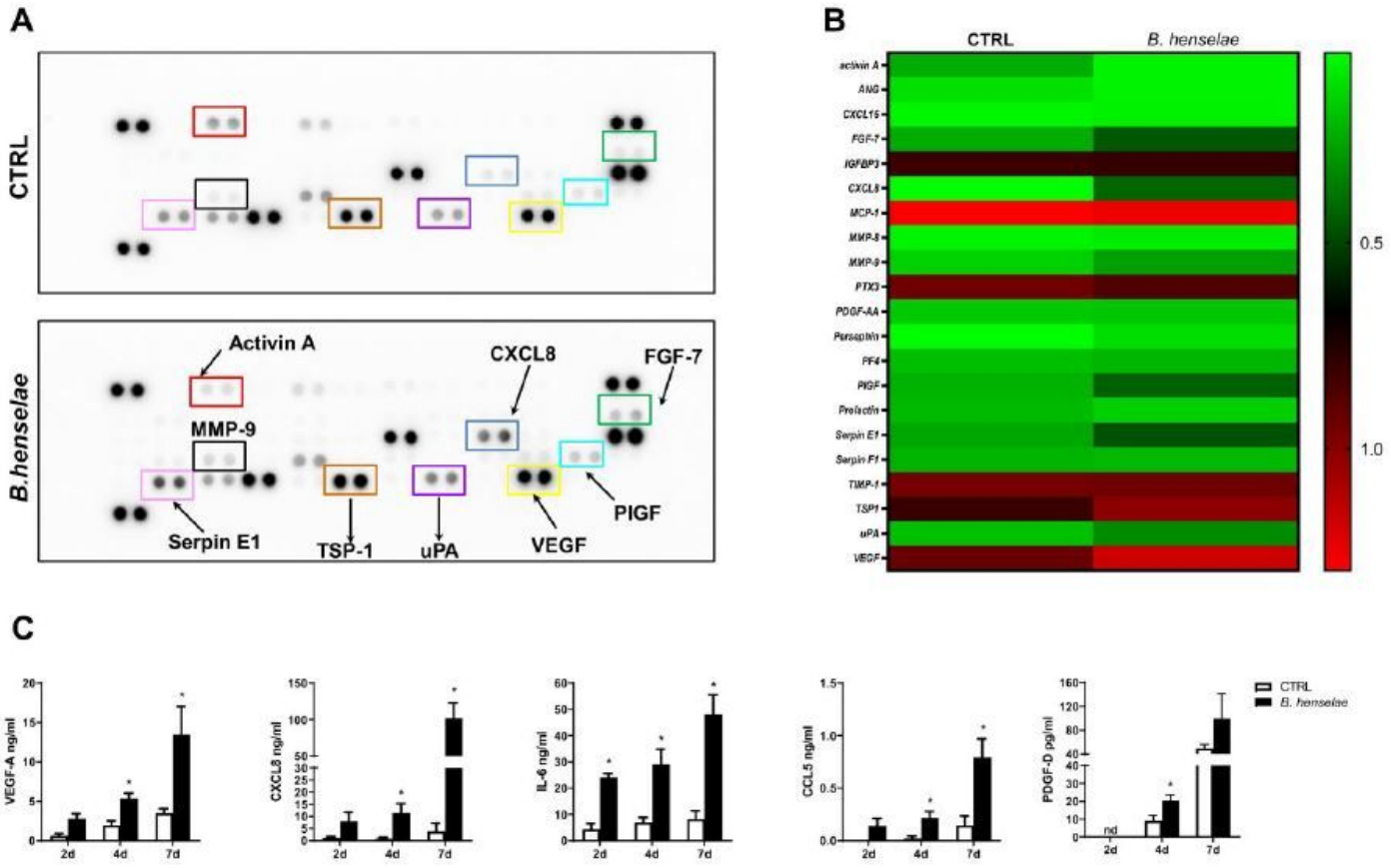

Figure 6

Angiogenic signature of B. henselae-infected MSCs. (A) Human angiogenesis antibody array analysis was performed using a pool of supernatants from 96 h uninfected MSC (CTRL) or B. henselae-infected MSCs. Some of the most representative angiogenic factors are highlighted in different colors. The graph with normalized pixel density of all the visualized spots is shown in Fig. S1 in the supplemental material. (B) Heat map analysis representing the normalized average pixel density of the pair of duplicate spots for each angiogenic-related protein in the array. (C) Quantification of VEGF-A, CXCL8, IL-6, CCL5 and PDGF-D production in uninfected (CTRL) and B. henselae-infected MSCs. Data are expressed as mean ± SEM of 3 independent experiments. * $P < 0.05$ vs CTRL; unpaired t-test. nd= not detectable.

Supplementary Files

This is a list of supplementary files associated with this preprint. Click to download.

- AdditionalFile1.pdf
- AdditionalFile1.pdf